Rapamycin Reduces Arterial Mineral Density and Promotes Beneficial Vascular Remodeling in a Murine Model of Severe Medial Arterial Calcification.

Parya Behzadi[1], Rolando A. Cuevas[1], Alex Crane[1], Andrew A Wendling[1], Claire C. Chu[1], William J Moorhead III[1], Ryan Wong[1], Mark Brown[1], Joshua Tamakloe[1], Swathi Suresh[1], Payam Salehi[2], Iris Z. Jaffe[3], Allison L. Kuipers[4], Lyudmila Lukashova[5], Konstantinos Verdelis[5], and Cynthia St. Hilaire[1,6,7]

[1] Department of Medicine, Division of Cardiology, and the Pittsburgh Heart, Lung, Blood and Vascular Medicine Institute, University of Pittsburgh, Pittsburgh, Pennsylvania, USA.

[2] CardioVascular Center, Vascular Surgery, Tufts Medical Center, 800 Washington Street, Boston, MA, 02111-1800, USA

[3] Molecular Cardiology Research Institute, Tufts Medical Center, 800 Washington Street, Boston, MA, 02111-1800, USA

[4] Department of Epidemiology, School of Public Health, University of Pittsburgh, Pittsburgh, Pennsylvania, USA

[5] Departments of Endodontics and Oral Biology, School of Dental Medicine, University of Pittsburgh, Pittsburgh, PA, USA

[6] Department of Bioengineering, University of Pittsburgh, Pittsburgh, Pennsylvania, USA

[7] Department of Cardiothoracic Surgery, University of Pittsburgh, Pittsburgh, Pennsylvania, USA

ABSTRACT: 251 words

MANUSCRIPT:

KEYWORDS: Medial Arterial Calcification, Rapamycin, Matrix GLA protein, Collagen, Elastin

ABBREVIATIONS

Adenosine monophosphate	AMP
Adenosine triphosphate	ATP
Alkaline phosphate	TNAP
Arterial calcification due to deficiency of CD73	ACDC
Ecto-5'-nucleotidase	NT5E
Induced pluripotent stem cells	iPSCs
Matrix GLA protein	MGP
Medial arterial calcification	MAC
mTORC complex 1	mTORC1
mTORC complex 2	mTORC2
Peripheral artery disease	PAD
Smooth muscle α-actin	SMA
Smooth muscle cells	SMCs
Myosin heavy chain 11	MYH11
Runt-related transcription factor 2	RUNX2

ABSTRACT

Peripheral artery disease (PAD) is the narrowing of the arteries that carry blood to the lower extremities. PAD has been traditionally associated with atherosclerosis. However, recent studies have found that medial arterial calcification (MAC) is the primary cause of chronic limb ischemia below the knee. MAC involves calcification of the elastic fibers surrounding smooth muscle cells (SMCs) in arteries. Matrix GLA protein (MGP) inhibits vascular calcification by binding circulating calcium and preventing hydroxyapatite crystal deposition, while also modulating osteogenic signaling by blocking BMP-2 activation of RUNX2. *Mgp*$^{-/-}$ mice develop severe MAC and die around 8 weeks after birth due to aortic rupture or heart failure. We previously discovered a rare genetic disease Arterial Calcification due to Deficiency in CD73 (ACDC) in which patients present with extensive MAC in their lower extremity arteries. Using a patient-specific induced pluripotent stem cell model we found that rapamycin inhibited calcification. Here we investigated whether rapamycin could reduce MAC in vivo using the *Mgp*$^{-/-}$ murine model. *Mgp*$^{+/+}$ and *Mgp*$^{-/-}$ mice received 5mg/kg rapamycin or vehicle. Calcification content was assessed via microCT, and vascular morphology and extracellular matrix content assessed histologically. Immunostaining and western blot analysis were used to examine SMC phenotype and extracellular matrix content. Rapamycin prolonged *Mgp*$^{-/-}$ mice lifespan, decreased mineral density in the arteries, maintained SMC contractile phenotype, and improved vessel structure, however, calcification volume was unchanged. *Mgp*$^{-/-}$ mice with SMC-specific deletion of Raptor or Rictor, did not recapitulate treatment with rapamycin. These findings suggest rapamycin promotes beneficial vascular remodeling in vessels with MAC.

INTRODUCTION

Peripheral artery disease (PAD) is the narrowing of blood vessels in the lower extremities due to inward remodeling or thrombotic occlusion, both of which cause chronic limb ischemia and often result in amputation of the lower leg (1). Traditionally atherosclerosis was the assumed cause of PAD however recent studies now show that medial arterial calcification (MAC) promotes inward remodeling, and stiffness related to medial dysplasia induces thrombosis (2-4). MAC is characterized by the progressive buildup of calcium and phosphate within the arterial walls and is typically not associated with lipid deposition, fibrous cap formation, or intimal hyperplasia (5). These structural features distinguish MAC from atherosclerosis and indicate that MAC is a distinct pathology driving adverse outcomes in PAD. Currently, there are no specific medical therapies that target the pathogenesis of PAD or MAC. Finding therapies that can prevent, stop, or even reverse MAC in PAD could greatly enhance the current standard of care.

Vascular calcification stems from the nucleation of calcium and phosphate into hydroxyapatite crystals and the release of pro-mineralizing matrix vesicles from osteogenic-like arterial smooth muscle cells (SMCs) that accumulate along the elastic lamina (6). Phosphate is a byproduct of the breakdown of extracellular adenosine triphosphate (ATP) to adenosine, generating inorganic phosphate at several points (7, 8). There are a number of genetic diseases that present with MAC which harbor inactivating mutations in the genes related to extracellular ATP metabolism (5). Patients with Arterial Calcification due to Deficiency of CD73 (ACDC, also known as CALJA, OMIM # 211800) harbor inactivating mutations in the *NT5E* gene, which encodes for the CD73 enzyme that metabolizes extracellular AMP to adenosine and inorganic phosphate. Key signatures of this disease are calcification nodules in the small joint capsules and MAC in the lower-extremity arteries that initiate along the elastic lamina (4, 9, 10). We previously found that a lack of CD73-mediated adenosine enhanced the expression and activity of tissue-nonspecific alkaline phosphatase (TNAP), a key enzyme that promotes calcification (11).

Matrix GLA protein (MGP) is a vitamin-K2-dependent protein with an unusual gamma-carboxylation of five glutamate residues that enhance its affinity for calcium, preventing it from mineralizing (12). MGP also inhibits calcification propagation by binding to hydroxyapatite crystals and stimulating their uptake by local phagocytosing macrophages (13). MGP also modulates osteogenic signaling by binding to BMP-2, preventing it from activating receptors and upregulating RUNX2, the key regulator of osteoblast differentiation and maturation (14, 15). Mice that lack MGP develop to term but die prematurely within approximately two months of age due to extensive MAC, which leads to aortic rupture or heart failure (16). Aortas of MGP-deficient mice exhibit increased collagen accumulation and elastic fiber fragmentation within the medial layer of the arteries where calcification is also localized. This is phenotypically similar to MAC observed in human patients with PAD MAC and ACDC patients (4).

The drug rapamycin inhibits the mammalian target of rapamycin (mTOR), a protein kinase broadly expressed throughout the body, which controls many key processes such as energy balance, autophagy, and proliferation (17-20). Rapamycin protects against the calcification of vascular cells in in vitro and ex vivo models, as well as in in vivo models of chronic kidney disease-induced MAC (21-23). We previously found rapamycin prevented calcification in in vitro and in vivo disease models of ACDC patient-specific induced pluripotent stem cells (iPSCs) (11).

While CD73-deficient humans develop extensive MAC in their lower extremity large vessels, CD73-deficient mice do not phenocopy humans and do not exhibit calcification in their vasculature (24, 25). As the MAC observed in MGP-deficient mice mirrors that seen in ACDC patients, we sought to investigate whether rapamycin prevented calcification in this genetic mouse model of MAC.

MATERIALS AND METHODS

Availability of Materials

We abide by the NIH Grants Policy on Sharing of Unique Research Resources, including the NIH Policy on Sharing of Model Organisms for Biomedical Research (2004), NIH Grants Policy Statement (2003), and Sharing of Biomedical Research Resources: Principles and Guidelines for Recipients of NIH Grants and Contracts (1999), and the Bayh-Dole Act and the Technology Transfer Commercialization Act of 2000. Materials generated in our laboratory are made available for non-commercial research per established University of Pittsburgh Office of Research IRB and MTA protocols.

Institutional Review Board Statement

De-identified human tissues were obtained, with informed consent from subjects, who were enrolled in studies approved by the University of Pittsburgh or Tufts Medical Center institutional review boards, per the Declaration of Helsinki.

Animals and cell line generation

Animal use was approved by the Institutional Animal Care and Use Committee at the University of Pittsburgh. MGP heterozygous mutant mice from a C57BL/6J background (strain# 023811 Jackson Laboratory, Bar Harbor, ME) were bred to produce +/+ and -/- littermate controls. Smooth muscle lineage-specific *Raptor* (*Mgp*$^{-/-}$; *Raptor*$^{SMC-/-}$) and *Rictor* (*Mgp*$^{-/-}$; *Rictor*$^{SMC-/-}$) knockout mice were produced by breeding *Mgp*$^{+/-}$ with Myh11-Cre-eGFP mice (strain# 007742 Jackson Laboratory, Bar Harbor, ME)(26), with Raptor-LoxP (strain# 013188 Jackson Laboratory, Bar

Harbor, ME)(27), or *Rictor*-LoxP (strain# 020649 Jackson Laboratory, Bar Harbor, ME)(28). Genotypes were determined from tail snips that were incubated in DirectPCR Lysis Reagent (Viagen Biotech) according to manufacturer instructions. The lysate was amplified using OneTaq MasterMix (New England Biolabs) according to manufacturer instructions with primers suggested by Jackson Laboratories. The PCR reaction was run on an ethidium bromide agarose gel. SMC were obtained from three- to five-week-old male and female $Mgp^{+/+}$ and $Mgp^{-/-}$ mice.

Cell culture

$Mgp^{+/+}$ and $Mgp^{-/-}$ aortic SMC lines from male and female murine aorta were cultured in Dulbecco's modified Eagle's medium (DMEM; Gibco, Waltham, MA) supplemented with 20% FBS (FBS; R&D Systems, Minneapolis, MN) and 100 U/mL penicillin-streptomycin (P/S; Gibco, Waltham, MA). Growth media was changed every three days, and cells were split 1:2 when confluent. Post-expansion, 25,000–50,000 cells/cm² were plated in DMEM supplemented with 10% FBS and 100 U/mL penicillin-streptomycin, and grown to confluence. Before all experiments/treatments, cells were serum-starved in DMEM with 0.5% FBS for 48 h. Incubation under reduced serum conditions has been proven to be a beneficial technique for studying smooth muscle cell remodeling and contractility in vitro (29, 30). Cells were treated with rapamycin (Novus Biologicals) at concentrations of 200 nM or the same volume of DMSO as vehicle control for 14h. For autophagy flux assessment, cells were exposed to either bafilomycin A1 100 nM (Sigma-Aldrich) or rapamycin 200 nM for a duration of 24h following treatment intervention. All chemicals were dissolved in DMSO and administered in equal volume as vehicle control.

Tissue Extraction

Mice were sacrificed by asphyxiation with carbon dioxide, followed by perforation of the diaphragm. Tissue extraction began with dissection through the abdominal wall and then perfusion of the heart with 50 mL of DPBS supplemented with 1:100 Amphotericin B (15290026, Gibco) and 1:200 Gentamicin (15710064, Gibco). The aortas were maintained in this solution while the adventitia was removed in a petri dish. Tissues were then fixed in 4% paraformaldehyde in PBS for 2 hours and then placed in PBS. Tissues were brought to microCT and then embedded in paraffin, or embedded in paraffin directly.

In Vivo Rapamycin Injections

Male and female $Mgp^{-/-}$ mice received intraperitoneal injections of either vehicle or 5 mg/kg rapamycin dissolved in 0.3 mg/ml peanut oil once a week beginning at 10 days of age. This process continued until the natural death of all mice in each group. To assess the volume and density of calcification, male and female $Mgp^{-/-}$ mice received intraperitoneal injections of either vehicle, 1x/week rapamycin or 3x/week rapamycin from 10 to 25 days of age.

Micro-Computed Tomography

A Scanco 30μCT microCT scanner (Scanco Medical, Basserssdorf, Switzerland) with a 45 kVp beam energy (1,000 ms exposure) was used to assess the volume and density of calcification in mouse aorta ex vivo, as previously described (11, 31). No filtering was used, allowing for visibility of lower CT densities. Images were then analyzed for relative calcified mass within the aorta (expressed as bone volume fraction) using the Scanco 3D Morphometry and Densitometry Analysis software (Scanco Medical) after binarization of the images with a global threshold within a user-defined aorta region of interest.

Western Blot Analysis

Cells were lysed in 1% CHAPS hydrate, 150 mmol/L sodium chloride, 25 mmol/L HEPES buffer supplemented with 1× protease and phosphatase inhibitor (Sigma-Aldrich). Cells were scraped into microcentrifuge tubes, vortexed for 5 minutes, freeze/thawed for 5 to 8 cycles, then centrifuged at 12 000×g for 10 minutes at 4°C. Supernatant protein concentration was determined using Pierce BCA protein assay kit (Thermo Fisher, Waltham, MA). Ten micrograms of protein were used in the preparation of lysate with 1 × Pierce LDS sample buffer nonreducing (Thermo Fisher, Waltham, MA) and 1 × NuPAGE sample reducing agent (Novex, Waltham, MA). Lysates were denatured at 95°C for 15 min and then electrophoresed on 4%–20% TGX stain-free polyacrylamide gel (Bio-Rad, Hercules, CA) in 1 × Tris/Glycine/SDS buffer (Bio-Rad, Hercules, CA) at 120 V for 50 min. Protein was transferred onto a 0.2 μm nitrocellulose membrane in prepared 1 × Towbin buffer with ethanol (EtOH) at 1 A and 25 V for 30 min using the Trans-Blot Turbo Transfer System (Bio-Rad, Hercules, CA). Membranes were blocked in 1:1 Odyssey blocking buffer (Li-COR, Lincoln, NE) and PBS for 1 h at room temperature, followed by primary antibody incubation in 1:1 Odyssey blocking buffer and PBS plus 0.1% Tween 20 (PBS-T) at 4°C overnight. Membranes were washed in PBS-T three times for 5 min, then incubated in secondary antibody at room temperature for 1 h. Membranes belonging to the same experimental set were imaged simultaneously on an Odyssey CLx (LI-COR, Lincoln, NE), and band intensity quantification was performed with Image Studio (Version 5.2, LI-COR, Lincoln, NE) software. Individual bands were normalized to α-tubulin, and each treatment group's fold change was compared with each gel's vehicle control lanes. For sequential antibody incubations, membranes were stripped in 1 × NewBlot Nitro Western Blot Stripping Buffer (LI-COR, Lincoln, NE) for 10 min, followed by three washes in PBS.

Verhoeff Van Gieson, Von Kossa, Masson's Trichrome and Picrosirius Red Staining

Mice aortic tissues were removed from mice through the abdominal wall under anesthesia conditions. Then aortic tissue was fixed with 4% paraformaldehyde and embedded in paraffin. The embedded specimens were transversely sectioned at 10 μm on a microtome cryostat (Microm HM 325). Slides with the adhered paraffin aortic sections were warmed to 65°C for 1 h and then deparaffinized through xylene, rehydrated with serial incubation in graded alcohol baths, and stained with Verhoeff–van Gieson for elastic fiber visualization (Polysciences, 25089-1), Von Kossa for calcification (Polysciences, 24633-1), Masson's for collagen fibers (Polysciences, 25088-1) and Picrosirius Red staining for collagen quantification according to manufacturer's instructions. Verhoeff Van Gieson, Von Kossa, Masson's Trichrome images were captured using PreciPoint scanner. Collagen staining was assessed by measuring the intensity of collagen in the vessel wall normalized to scale bar. Picrosirius Red staining images were captured collagen with the Olympus VS200 Slide Scanner. The percentage of medial thickness of the medial layer was measured using ImageJ software (Java 8), where the medial thickness was determined by measuring the distance between the inner and outer elastic lamina at four sites per vessel. The percentage of calcification in the medial layer was measured using ImageJ software (Java 8) where the area of calcification was normalized to total medial area. The tortuosity of elastic fibers was measured by selecting three representative areas with the whole vessel. ImageJ was used to trace and measure the length of five elastic fibers and shown as a ration over the vessel length. The number of breakages in the elastic lamina was assessed by counting the breaks throughout the entire aorta. All length measurements were normalized to the scale bar units.

Immunofluorescence

Slides with the adhered paraffin aortic sections were warmed to 65°C for 1 h and then deparaffinized through xylene, rehydrated with serial incubation in graded alcohol baths. Slides were boiled in citric acid-based antigen retrieval solution (H-3300, Vector Labs) for 20 minutes.

Slides were cooled in the unmasking solution for 1 hour, washed in 1x PBS and placed in blocking buffer (500 mL PBS 0.3g Fish Skin Gelatin) for 1 hour. Tissues were incubated overnight at 4°C with antibodies for ACTA2 (Abcam, ab5694, 1:50), Ki67 (Abcam, ab15580, 1:250), LC3 (cell signaling,124714, 1:50), MGP (10734-I-AP, 1:25), MYH11 (Invitrogen, MA5-4284, 1:50) , RUNX2 (ABclonal, A2851, 1:100). All signals were optimized to IgG (Vector, 31235, 1:50). Cells were washed 3× for 5 minutes each with PBS, 0.1% TWEEN 20, then once with PBS, and then incubated with secondary antibody (A11006, A11012, Thermo Fisher) for 1 hour. Cells were washed 3× for 5 minutes each with PBS, 0.1% TWEEN 20, then once with PBS, then mounted with Fluoroshield Mounting Medium with DAPI (Ab104139, Abcam). Slides were imaged within 24 hours of mounting. Cells were imaged within 24 hours of mounting. In ImageJ, each image was split into blue, red, and green channels, and the pixel intensity of the red and blue channels was measured (32). The measured intensity of a given stain was normalized to DAPI intensity of that same image. We obtained the von Kossa staining images using PreciPoint scanner and the immunofluorescent image using a Nikon NI-E I microscope.

Statistics

Statistical analysis was performed with GraphPad Prism 9.2 (GraphPad Software, Inc) and data shown are mean±SD. Statistical significance between groups was assessed using the Kruskal Wallis test or by Two-way ANOVA according to the data set. Statistical analysis used, exact n values, biological replicates, and P values are stated within each figure legend. A p-value equal to or less than 0.05 will be considered statistically significant.

RESULTS

MAC in MGP-deficient mice phenocopies human MAC.

The main characteristic of MAC is calcification in the media along the elastic lamina. Von Kossa staining for calcification illustrates that *Mgp*$^{-/-}$ mouse aortas have extensive mineralization in the medial layer, which phenocopies the mineralization seen in MAC of the human tibial arteries and is distinct from neointimal calcification found in the necrotic core of coronary artery with atherosclerotic plaque (Figure 1A). MGP is a potent inhibitor of soft tissue calcification. *Mgp*$^{-/-}$ mice do not produce functional MGP protein (Figure 1B, 1C) and, as a result, develop extensive MAC pathology in large vessels (16).

Rapamycin reduces mineral density in *Mgp*$^{-/-}$ mice.

Humans with inactivating mutations in *NT5E* develop extensive MAC in their lower extremity arteries (9). It has been shown that the *Nt5e*-knockout mice model shows altered renal function, diminished control of the glomerular arteriolar tone, elevated atherogenesis, elevated thrombotic occlusion, and elevated hypoxia-induced vascular leakage (24), these mice do not mimic the human vascular calcification phenotype (24, 25, 33). Jin et al. circumvented this issue using a patient-specific in vitro and in vivo disease modeling system using iPSC technology. They demonstrated that patient-specific ACDC-iPSCs developed extensive calcification in the in vivo teratoma model relative to control patient iPSCs. Furthermore, they found that treating mice bearing ACDC-iPSC teratomas with rapamycin reduced calcification (11).

As CD73-deficient mice do not sufficiently recapitulate the MAC observed in ACDC patients, we used the *Mgp*$^{-/-}$ mice as an in vivo model of MAC to test the hypothesis that rapamycin could reduce vascular calcification in vivo. *Mgp*$^{+/+}$ and *Mgp*$^{-/-}$ mice were administered 5 mg/kg rapamycin of the same volume of vehicle (DMSO) three times per week starting at 10 days old until natural death (Figure 2A). We discovered that rapamycin treatment extended the lifespan of *Mgp*$^{-/-}$ mice

292 (T_{50} 61 days) compared to the *Mgp*$^{-/-}$ mice treated with the vehicle (T_{50} 35 days), which start to die
293 as early as day 20 (Figure 2B). Both male (n=11) and female (n=8) were used however no sex
294 differences were observed between *Mgp*$^{-/-}$ mice that had received either vehicle or rapamycin
295 treatment.
296
297 We next investigated whether calcification content was altered in mice receiving rapamycin. Mice
298 received vehicle, one dose of 5 mg/kg rapamycin per week, or 5 mg/kg rapamycin three times a
299 week. Mice were sacrificed at day 25 and mineral was assessed via microCT (Figure 3A). We
300 selected this time point because we observed that the mice began dying at 25 days (Figure 2B).
301 Whole aorta microCT analysis found no differences in the total calcification volume under either
302 treatment regime; however, mice receiving a rapamycin 3x per week exhibited decreased mineral
303 density compared to the control group (Figure 3B). Based on this data, we proceeded with
304 3x/week for the rest our studies. Von Kossa stain showed that the aortas of *Mgp*$^{+/+}$ mice exhibit
305 no mineralization, while both vehicle- and rapamycin-treated *Mgp*$^{-/-}$ mice showed extensive
306 calcification compared to *Mgp*$^{+/+}$ mice, there were no discernible differences in the calcified area
307 or the medial thickness vehicle or rapamycin groups of *Mgp*$^{-/-}$ (Figure 3C). RUNX2 is a key
308 transcription factor promoting vascular cell osteogenic differentiation (6). Immunofluorescent
309 staining revealed that while *Mgp*$^{-/-}$ mice showed elevated levels of RUNX2 compared to *Mgp*$^{+/+}$
310 mice, however rapamycin treatment did not reduce RUNX2 expression in *Mgp*$^{-/-}$ compared to *Mgp*
311 $^{-/-}$ treated with vehicle (Figure 3D). These findings suggest that while rapamycin doubles the
312 lifespan of *Mgp*$^{-/-}$ mice, it does not lead to decreased calcification volume, but does promote les-
313 dense mineral formation in *Mgp*$^{-/-}$ mice.
314
315 **Rapamycin alters SMC phenotype and ECM content in vivo**
316 The drug rapamycin has a broad spectrum of effects on SMCs. Rapamycin inhibits SMC migration
317 and proliferation by inducing the cyclin-dependent kinase inhibitors $p27^{kip}$ and $p21^{cip}$ and
318 promotes G1-S cell cycle arrest (34, 35). Rapamycin also induces SMC differentiation by inhibiting
319 the mTOR-target S6K1 via AKT activation, promoting SMC contractile phenotype by enhancing
320 SMA and MYH11 protein expression (36). Further, rapamycin was shown to protect against
321 calcification of vascular cells in in vitro and ex vivo models (11, 21). While rapamycin did not
322 reduce calcification volume in *Mgp*$^{-/-}$ vessels we hypothesized that it could perhaps prevent aortic
323 rupture by maintaining SMC contractile phenotype or stabilize the ECM.
324
325 Masson's trichrome staining shows that *Mgp*$^{-/-}$ vehicle vessels are highly remodeled, with acellular
326 areas exhibiting observable increased collagen staining (Figure 4A). Picrosirius staining enabled
327 quantification of collagen content and shows that, while not at the levels seen in *Mgp*$^{+/+}$ vessels,
328 rapamycin increased the collagen content in the vessels of *Mgp*$^{-/-}$ mice (Figure 4B). This suggests
329 that rapamycin helps restore or stabilize the collagen within the ECM, which is likely offering a
330 protective effect by strengthening tissue structure to improve resilience against rupture. Verhoeff-
331 Van Gieson (VVG) staining revealed that the aortas of *Mgp*$^{-/-}$ mice exhibited less robust staining
332 for elastin, and less tortuous fibers, in *Mgp*$^{-/-}$ compared to *Mgp*$^{+/+}$. While rapamycin did not alter
333 elastic fiber tortuosity in *Mgp*$^{-/-}$ mice compared to vehicle controls, the number of elastin breakages
334 was higher in *Mgp*$^{-/-}$ mice compared to *Mgp*$^{+/+}$ in both groups, and rapamycin treatment reduced
335 the number of breakages in *Mgp*$^{-/-}$ mice compared to vehicle (Figure 4C).
336
337 Immunofluorescent staining was used to quantify the SMC contractility markers smooth muscle
338 α-actin (SMA) and myosin heavy chain 11 (MYH11) (37, 38). In *Mgp*$^{+/+}$ we observed no differences
339 in SMA levels between vehicle and rapamycin treatment, nor between *Mgp*$^{+/+}$ the *Mgp*$^{-/-}$ mice
340 treated with vehicle. However, rapamycin treatment slightly, but significantly, increased SMA

levels in *Mgp*$^{-/-}$ mice compared to vehicle alone. No differences in MYH11 levels were observed (Figure 4D). These results suggest a slight increase in the contractile phenotype of SMCs of *Mgp*$^{-/-}$ mice treated with, but not to levels see in *Mgp*$^{+/+}$ mice. As the medial layer is remodeled in the *Mgp*$^{-/-}$ mice, we also measured the mitotic marker Ki67 and found that at baseline, Ki67 levels were significantly elevated in *Mgp*$^{-/-}$ aorta while nearly undetectable in the *Mgp*$^{+/+}$. However, rapamycin treatment did not alter Ki67 levels in either of the two genotypes (Figure 4E). Together, these data suggest that rapamycin does not significantly alter the medial remodeling or SMC phenotype in *Mgp*$^{-/-}$ mice aorta.

Rapamycin lowered LC3 staining in *Mgp*$^{-/-}$ aorta but there were no observable changes in autophagy flux.

Autophagy is a ubiquitous process and contributes to bone development and the differentiation of osteoblasts and osteoclasts (39) One study found that autophagy reduces vascular calcification by limiting the release of pro-calcific matrix vesicles (40). Another found that in vitro, autophagy stimulation with valproic acid protects against phosphate-induced calcification, while its inhibition increases extracellular vesicle release in SMCs (23). LC3 is a protein that functions at the initiation of autophagosome formation and serves as an autophagy marker. While there were no differences between the LC3 signal in *Mgp*$^{+/+}$ and *Mgp*$^{-/-}$ at baseline, we observed that rapamycin treatment significantly lowered LC3 puncta in *Mgp*$^{-/-}$ compared to *Mgp*$^{+/+}$ mice (Figure 5A).

Quantifying LC3 puncta hints at diminished autophagy, but immunofluorescent staining of fixed tissues cannot assess autophagy flux because it provides only a single snapshot of the autophagic process, which does not reflect changes in the dynamic turnover of autophagosomes or the lysosomal clearance of LC3-positive autophagic vesicles. LC3-I is cleaved to LC3-II when it is incorporated into autophagosomes, but this process is dynamic, and LC3-II can also be degraded during autophagy. The comparison of LC3-II to LC3-I in the presence of an autophagy inhibitor like bafilomycin enables autophagy flux observation (41). We isolated SMCs from *Mgp*$^{+/+}$ and *Mgp*$^{-/-}$ mice to evaluate autophagy flux. SMC were treated with vehicle (DMSO) or 200 nM rapamycin for 14h and then with vehicle or 100 uM or the late-phase autophagy inhibitor bafilomycin for 24h. Rapamycin alone did not increase LC3-II levels compared to vehicle controls in either the *Mgp*$^{+/+}$ and *Mgp*$^{-/-}$ SMC. Bafilomycin, an autophagy inhibitor, increased LC3-II levels in both *Mgp*$^{+/+}$ and *Mgp*$^{-/-}$ SMCs compared to their cognate vehicle controls, however the addition of rapamycin did not further alter LC3-II levels compared to bafilomycin (Figure 5B, left graph). Comparing LC3-II to LC3-I showed identical trends (Figure 5B, right graph), suggesting that global LC3 levels and flux are similar in *Mgp*$^{+/+}$ and *Mgp*$^{-/-}$ SMCs.

Genetic deletion of mTOR signaling in the SMCs does not replicate rapamycin treatment *Mgp*$^{-/-}$ mice.

Figure 2 shows that rapamycin treatment doubles the lifespan of *Mgp*$^{-/-}$ mice compared to vehicle alone. However, our subsequent inquiries revealed that rapamycin did not decrease the volume of calcification, as was seen in in vivo iPSC teratoma models (11), while it did promote less dense mineral formation, and beneficial SMC phenotype and EMC remodeling, albeit not to levels seen in the *Mgp*$^{+/+}$ animals. The mammalian target of rapamycin, mTOR, can form two different protein complexes known as mTORC1, bound to Raptor, and mTORC2, bound to Rictor. The former is acutely sensitive to rapamycin administration, while the latter requires chronic rapamycin dosing for inhibition (19). To investigate whether rapamycin's effects on the *Mgp*$^{-/-}$ mouse are acting through either of these complexes, we generated *Mgp*$^{-/-}$ mice with SMC-specific deletion of the mTOR complex proteins Raptor and Rictor (26-28). *Mgp*$^{-/-}$*;Myh11Cre-GFP;Raptor*$^{f/f}$ mice (*Mgp*$^{-/-}$*;Raptor*$^{SMC-/-}$) were bred to examine the effects of a nonfunctional mTORC1 complex, while *Mgp*$^{-}$

390 $^{-/-}$;*Myh11Cre-GFP;Rictor*$^{f/f}$ (*Mgp*$^{-/-}$;*Rictor*$^{SMC-/-}$) mice knockout was bred to examine a nonfunctional
391 mTORC2 complex. Fully differentiated SMCs expressing *Myh11* will constitutively express Cre
392 recombinase to inactive *Raptor* and *Rictor* gene expression specifically in SMCs.
393
394 Similar to *Mgp*$^{-/-}$ mice treated with vehicle in Figure 2, Figure 6 shows that only 50% of the *Mgp*$^{-/-}$
395 ;*Rictor*$^{SMC-/-}$ and *Mgp*$^{-/-}$;*Rictor*$^{SMC+/+}$ are alive at 40 days, indicating that rapamycin acting via
396 mTORC2 does not recapitulate the effects of rapamycin on increasing *Mgp*$^{-/-}$ mice lifespan. The
397 50% survival rate of *Mgp*$^{-/-}$;*Raptor*$^{SMC+/+}$ mice was similar to *Mgp*$^{-/-}$ treated with vehicle, *Mgp*$^{-/-}$
398 ;*Rictor*$^{SMC-/-}$ and *Mgp*$^{-/-}$;*Rictor*$^{SMC+/+}$, however the 50% survival rate of MGP$^{-/-}$;Raptor$^{SMC-/-}$ mice
399 dropped to 22 days. As the Cre strain being used is a non-inducible system, this data in the MGP^{-}
400 $^{/-}$;Raptor$^{SMC-/-}$ mice suggest that mTORC1 is critical to the growth and development of the
401 vasculature. Together, these in vivo data suggest that the life-extending effects of rapamycin in
402 the *Mgp*$^{-/-}$ mouse are not acting through the mTORC2 complex. Additional experiments, such as
403 a tamoxifen inducible Cre system, would need to be used to fully address the contribution of
404 mTORC1 to mirror effects seen by rapamycin injection.
405
406 **DISCUSSION**
407 In this study, we demonstrated that rapamycin treatment increased the lifespan in *Mgp*$^{-/-}$ mice, but
408 the effects of rapamycin do not reduce MAC. In mice, rapamycin has been shown to increase
409 maximum lifespan and delay the onset of cancer as hyperactivity of the mTOR pathway,
410 frequently found in cancers, leads to the expression and activation of many oncogenes like PI3K,
411 Akt, and eIF4E. Hence, rapamycin can slow the proliferation of tumor cells by causing cell arrest,
412 promoting apoptosis, and blocking angiogenesis in tumor growths (42). Our data show that the
413 increase in lifespan observed in *Mgp*$^{-/-}$ mice following rapamycin treatment is associated with
414 improvements in SMC contractile protein expression and collagen content in the vessel wall, but
415 not with enhanced autophagy flux.
416
417 Collagen, the most abundant protein in the ECM, plays a crucial role in maintaining the structural
418 integrity of the blood vessels. Collagen degradation leads to increased vessel distensibility and
419 the risk of rupture (43, 44). Aging mice homozygous for a deletion in the gene coding for collagen
420 alpha 1(Col1a1) are at a significantly increased risk of aortic dissection and rupture (45). The
421 increase in collagen content observed in *Mgp*$^{-/-}$ mice treated with rapamycin compared to those
422 receiving vehicle treatment. The increase in collagen content following rapamycin treatment and
423 the increase in SMC contractile protein SMA may contribute to the prolonged lifespan of *Mgp*$^{-/-}$
424 mice by improving both the structural stability and functional resilience of the vascular walls.
425
426 While rapamycin is known to inhibit SMC proliferation and is used as such in drug-eluting stents,
427 there is limited research on the effects of rapamycin on vascular morphology in the presence of
428 calcification (35, 46). It was previously shown that treatment with rapamycin limits the progression
429 of abdominal and thoracic aortic aneurysms in mice and preserves elastic lamina integrity (47,
430 48). In a hyperphosphatemic rat model, rapamycin treatment inhibited aortic calcium deposition
431 when ectopic calcification was induced by feeding the rats with a high-phosphate, high-adenine
432 diet. Rapamycin reduced the osteogenic markers MSX2 and OSX in this model while increasing
433 the *Opn* and *Acta2* gene expression via Klotho upregulation (49). Our approached used a genetic
434 model of MAC to investigate whether rapamycin could inhibit calcification in vivo. MGP-deficient
435 mice develop normally and at the time of birth are without any overt abnormalities. At
436 approximately one week old *Mgp*$^{-/-}$ mice start exhibiting calcification of the vessels, suggesting
437 that other gene products might compensate to prevent calcification during development and
438 immediately post-birth (16). These observations highlight the differences between genetically

439 induced MAC and high phosphate feeding models. Diet-induced calcification must overcome the
440 effect of endogenous MGP, which is a potent inhibitor of calcification, while the genetic removal
441 of MGP results in calcification from the circulating calcium and phosphate and activation of BMP
442 signaling (12, 15).
443
444 Rapamycin has also been shown to preserve the differentiated phenotype of vascular SMCs
445 through IRS-1/P3K/AKT2 pathway (36). Our study did observe rapamycin enhancing expression
446 of a SMC contractile protein in *Mgp*$^{-/-}$ mice. *Sma* expression typically occurs earlier than *Myh11*
447 expression during SMC development (50). In contrast, *Myh11* expression occurs later, during the
448 maturation of SMCs. The first study examined SMC contractile gene expression in response to
449 rapamycin in vitro (36), while our study looked at the SMC contractile markers in vivo. Further,
450 the presence of calcification activates mechanosensing pathways that once activated may
451 prevent full re-expression SMC contractile markers (51). However, further investigation is needed
452 to elucidate how these mechanisms are operating in the context of the *Mgp*$^{-/-}$ mouse.
453
454 MAC is characterized by mineral deposits in the medial vessel layer and frequently occurs in
455 patients with PAD. Vascular calcification is an active biological process with many driving forces,
456 including osteogenic dedifferentiation of SMCs, inflammatory signals, hyperphosphatemia, and
457 extracellular matrix remodeling. In this study, rapamycin prolonged the lifespan of mice who
458 developed significant MAC shortly after birth. Interestingly, even though rapamycin stimulates the
459 cellular process of autophagy (52)—which can recycle components of the ECM, including mineral
460 deposits (53)–calcification volume was not reduced in rapamycin treated *Mgp*$^{-/-}$ mice. However,
461 microCT data showed that the mineral density was significantly reduced in *Mgp*$^{-/-}$ mice treated
462 with rapamycin. The decrease in mineral density without a change in calcification volume could
463 suggests a shift from dense, organized macrocalcifications to more dispersed calcium-rich
464 extracellular vesicles and amorphous calcium phosphate deposits (7, 54). Amorphous calcium
465 phosphate, primarily composed of calcium and phosphate ions, represents the early stages of
466 calcification (55). It subsequently acts as a precursor for the nucleation and growth of
467 hydroxyapatite crystals within the ECM. Stabilization of hydroxyapatite crystals further contribute
468 to the transition into a bone-like phenotype. One reason that a lower mineral density did not affect
469 total calcification volume could be a difference in the pattern of mineral deposition. For example,
470 the mineral may form in a less compact, more porous manner, leading to a lower overall density
471 despite occupying the same spatial volume. Alternatively, the reduction in density could result
472 from the breakdown, or remodeling of pre-existing mineral deposits. This suggests that changes
473 in mineral structure, if explored at a further timepoint, may impact calcification volume.
474 Alternatively, as MGP also functions to inhibit BMP2 signaling, rapamycin may not interfere with
475 that process, such that changes in dosage or duration of rapamycin treatment would still not alter
476 calcification content in the vessel wall. Another explanation is that the activated autophagy
477 pathways cannot overcome the rapid deposition of hydroxyapatite that occurs in *Mgp*$^{-/-}$ mice.
478 Frauscher et al. demonstrated that induction of autophagy by rapamycin treatment decreased
479 calcification in the vasculature of uremic DBA/2 mice (56). This argument led us to examine
480 autophagy flux in SMCs. However, we did not observe a difference in autophagy flux between
481 *Mgp*$^{+/+}$ and *Mgp*$^{-/-}$. It is important to note that the *Mgp*$^{-/-}$ is on a C57BL6J background, perhaps
482 explaining the differences observed in these in vivo models.
483
484 It is said that rapamycin is an inhibitor of mammalian target of rapamycin (mTOR), but there is
485 more complexity to that. mTOR forms two distinct protein complexes known as mTORC1 and
486 mTORC2. mTORC1, activated by amino acids and allosterically inhibited by rapamycin, requires
487 a complex specific protein named raptor (57). mTORC1 is acutely sensitive to rapamycin, while

488 only after prolonged rapamycin treatment (>6 hours) does mTORC2 acquires a sensitivity to
489 rapamycin (20, 58). In the *Mgp*$^{-/-}$*;Raptor*$^{SMC-/-}$ mice, induction of Cre to knockout *Raptor* was more
490 lethal than the *Mgp*$^{-/-}$*;Raptor*$^{SMC+/+}$ or *Mgp-/-* mice. This suggests that *Raptor* is essential for the
491 growth and maintenance of SMCs in the vasculature. This essential role in growth and
492 development is perhaps unsurprising, considering that global *Raptor* knockout mice die in utero
493 (59). Moreover, there was no benefit to lifespan in the the *Mgp*$^{-/-}$:Rictor$^{SMC-/-}$ mice. The survival
494 curves for the the *Mgp*$^{-/-}$*:Rictor*$^{SMC+/+}$ and *Mgp*$^{-/-}$*;Rictor*$^{SMC-/-}$ mice, targeting mTORC2 signaling, do
495 not diverge at any point and are statistically insignificant, and also mirror that seen in the *Mgp*$^{-/-}$
496 strain.
497
498 Arterial stiffness is strongly linked to heart failure (60), and these non-atherosclerotic vascular
499 pathologies are much more common in some populations, such as African-ancestry individuals
500 who are known to have a higher risk of cardiovascular disease events and mortality compared to
501 Caucasians(61-65). This excess cardiovascular disease risk is largely due to hypertensive and
502 peripheral vascular disease, versus atherosclerotic disease (61-63, 66-68). As such, it is critical
503 to define drivers of MAC such as MGP, which in some clinical studies in humans has been
504 associated with heart failure and MAC (69). Impairment in MGP activation, which would
505 phenocopy genetic deletion, is linked to a higher risk of heart failure and peripheral artery disease
506 due to excessive pulsatile afterloads on the left ventricle that reduce coronary artery perfusion
507 pressure during diastole (70, 71). As the mice that lack MGP are prone to aortic rupture or heart
508 failure, we speculate that rapamycin's effect on the mice's lifespan may be due to rapamycin
509 acting on the cardiac tissues.
510
511 Our study suggests that rapamycin's life-extending benefit in *Mgp*$^{-/-}$ mice may act through
512 improvement in vascular function, which could prevent aortic rupture, or through another organ
513 system, possibly the heart. However, further studies are needed to examine the impact of
514 rapamycin on cardiac function in *Mgp*$^{-/-}$ mice. Rapamycin has been shown to increase
515 cardiomyocyte autophagy (72, 73), limit cardiomyocyte death, and attenuate cardiomyocyte
516 hypertrophy and cardiac remodeling by enhancing mTORC2 signaling while simultaneously
517 inhibiting mTORC1 signaling (74).Rapamycin had a protective effect on cardiomyocytes isolated
518 from the old mice compared to old mice not treated with rapamycin, as well as improved ejection
519 fraction, reduced cardiac hypertrophy and inflammation, and downregulated ANP-induced stress
520 response in vivo (75, 76). In mice with decompensated cardiac hypertrophy, rapamycin improved
521 cardiac function, such as left ventricular end-systolic dimensions, fractional shortening, and
522 ejection fraction in mice with compared to the control group (77). Three months of rapamycin
523 treatment in aged mice increased lifespan, decrease heart rate and heart weight (78). However,
524 a calcified phenotype was not noted in any of these animal studies.
525
526 **CONCLUSION**
527 This study provides novel insights into the effects of rapamycin on medial arterial calcification
528 (MAC) using the MGP-deficient murine model. While rapamycin did not reduce the volume of
529 calcification in the vasculature, it significantly prolonged the lifespan of *Mgp*$^{-/-}$ mice, possibly
530 through stabilizing vascular structure. This was evidenced by increased collagen content and
531 enhanced SMC contractile protein expression, which collectively suggest improved resilience
532 against vascular rupture. Interestingly, while the volume of calcification was not changed,
533 rapamycin treatment reduced mineral density. Further, our study underscores the importance of
534 distinguishing between mTORC1- and mTORC2-mediated pathways. Rapamycin's life-extending
535 effects appeared independent of autophagy flux or mTORC2 signaling, while the critical role of
536 mTORC1 in vascular development and maintenance was highlighted, as *Mgp*$^{-/-}$*;Raptor*$^{SMC-/-}$ died

earlier than *Mgp*$^{-/-}$ mice. These findings illustrate rapamycin's role in modifying calcification characteristics and enhancing vascular integrity without altering overall calcification volume. Future investigations should focus on elucidating rapamycin's systemic effects, such as its impact on cardiac function and/or the immune system, as well as understanding how it leads to less-dense mineral deposits, to clarify its protective mechanisms in the context of MAC and cardiovascular health.

ACKNOWLEDGEMENTS

We want to thank the histology core and the Center for Biologic Imaging at the University of Pittsburgh for their help and support with microscopy imaging. Some figures were created with Biorender.com.

SOURCES OF FUNDING

This publication was supported by the NIH K22 HL117917-01A1, The Winters Foundation, The McKamish Family Foundation (St. Hilaire), and the American Heart Association (Behzadi). MicorCT analysis and processing was performed on a system supported by NIH S10-OD021533 (Verdelis).

DISCLOSURES

None.

REFERENCES

1. **St Hilaire C**. Medial Arterial Calcification: A Significant and Independent Contributor of Peripheral Artery Disease. *Arterioscler Thromb Vasc Biol* 42: 253-260, 2022.
2. **O'Neill WC, Han KH, Schneider TM, and Hennigar RA**. Prevalence of nonatheromatous lesions in peripheral arterial disease. *Arterioscler Thromb Vasc Biol* 35: 439-447, 2015.
3. **Narula N, Dannenberg AJ, Olin JW, Bhatt DL, Johnson KW, Nadkarni G, Min J, Torii S, Poojary P, Anand SS, Bax JJ, Yusuf S, Virmani R, and Narula J**. Pathology of Peripheral Artery Disease in Patients With Critical Limb Ischemia. *J Am Coll Cardiol* 72: 2152-2163, 2018.
4. **Markello TC, Pak LK, St Hilaire C, Dorward H, Ziegler SG, Chen MY, Chaganti K, Nussbaum RL, Boehm M, and Gahl WA**. Vascular pathology of medial arterial calcifications in NT5E deficiency: implications for the role of adenosine in pseudoxanthoma elasticum. *Mol Genet Metab* 103: 44-50, 2011.
5. **Lanzer P, Hannan FM, Lanzer JD, Janzen J, Raggi P, Furniss D, Schuchardt M, Thakker R, Fok PW, Saez-Rodriguez J, Millan A, Sato Y, Ferraresi R, Virmani R, and St Hilaire C**. Medial Arterial Calcification: JACC State-of-the-Art Review. *J Am Coll Cardiol* 78: 1145-1165, 2021.
6. **Hortells L, Sur S, and St Hilaire C**. Cell Phenotype Transitions in Cardiovascular Calcification. *Front Cardiovasc Med* 5: 27, 2018.
7. **Villa-Bellosta R**. Role of the extracellular ATP/pyrophosphate metabolism cycle in vascular calcification. *Purinergic Signal* 19: 345-352, 2023.
8. **Rutsch F, Ruf N, Vaingankar S, Toliat MR, Suk A, Hohne W, Schauer G, Lehmann M, Roscioli T, Schnabel D, Epplen JT, Knisely A, Superti-Furga A, McGill J, Filippone M, Sinaiko AR, Vallance H, Hinrichs B, Smith W, Ferre M, Terkeltaub R, and Nurnberg P**. Mutations in ENPP1 are associated with 'idiopathic' infantile arterial calcification. *Nat Genet* 34: 379-381, 2003.

585 9. **St Hilaire C, Ziegler SG, Markello TC, Brusco A, Groden C, Gill F, Carlson-Donohoe**
586 **H, Lederman RJ, Chen MY, Yang D, Siegenthaler MP, Arduino C, Mancini C, Freudenthal**
587 **B, Stanescu HC, Zdebik AA, Chaganti RK, Nussbaum RL, Kleta R, Gahl WA, and Boehm**
588 **M**. NT5E mutations and arterial calcifications. *N Engl J Med* 364: 432-442, 2011.
589 10. **Baral A, F FH, Lee SC, Matthew BP, Ferrante EA, Brofferio A, Cudrici CD, Rollison**
590 **SF, Chen MY, Boehm M, and Wen H**. Images in Vascular Medicine: High-resolution CT
591 imaging of arterial calcification in the hands and legs of patients with CD73 deficiency. *Vasc*
592 *Med* 29: 342-344, 2024.
593 11. **Jin H, St Hilaire C, Huang Y, Yang D, Dmitrieva NI, Negro A, Schwartzbeck R, Liu**
594 **Y, Yu Z, Walts A, Davaine JM, Lee DY, Donahue D, Hsu KS, Chen J, Cheng T, Gahl W,**
595 **Chen G, and Boehm M**. Increased activity of TNAP compensates for reduced adenosine
596 production and promotes ectopic calcification in the genetic disease ACDC. *Sci Signal* 9: ra121,
597 2016.
598 12. **Murshed M, Schinke T, McKee MD, and Karsenty G**. Extracellular matrix
599 mineralization is regulated locally; different roles of two gla-containing proteins. *J Cell Biol* 165:
600 625-630, 2004.
601 13. **Hackeng TM, Rosing J, Spronk HM, and Vermeer C**. Total chemical synthesis of
602 human matrix Gla protein. *Protein Sci* 10: 864-870, 2001.
603 14. **Malhotra R, Burke MF, Martyn T, Shakartzi HR, Thayer TE, O'Rourke C, Li P,**
604 **Derwall M, Spagnolli E, Kolodziej SA, Hoeft K, Mayeur C, Jiramongkolchai P, Kumar R,**
605 **Buys ES, Yu PB, Bloch KD, and Bloch DB**. Inhibition of bone morphogenetic protein signal
606 transduction prevents the medial vascular calcification associated with matrix Gla protein
607 deficiency. *PLoS One* 10: e0117098, 2015.
608 15. **Bostrom K, Tsao D, Shen S, Wang Y, and Demer LL**. Matrix GLA protein modulates
609 differentiation induced by bone morphogenetic protein-2 in C3H10T1/2 cells. *J Biol Chem* 276:
610 14044-14052, 2001.
611 16. **Luo G, Ducy P, McKee MD, Pinero GJ, Loyer E, Behringer RR, and Karsenty G**.
612 Spontaneous calcification of arteries and cartilage in mice lacking matrix GLA protein. *Nature*
613 386: 78-81, 1997.
614 17. **Haissaguerre M, Saucisse N, and Cota D**. Influence of mTOR in energy and metabolic
615 homeostasis. *Mol Cell Endocrinol* 397: 67-77, 2014.
616 18. **Saxton RA, and Sabatini DM**. mTOR Signaling in Growth, Metabolism, and Disease.
617 *Cell* 168: 960-976, 2017.
618 19. **Panwar V, Singh A, Bhatt M, Tonk RK, Azizov S, Raza AS, Sengupta S, Kumar D,**
619 **and Garg M**. Multifaceted role of mTOR (mammalian target of rapamycin) signaling pathway in
620 human health and disease. *Signal Transduct Target Ther* 8: 375, 2023.
621 20. **Arriola Apelo SI, and Lamming DW**. Rapamycin: An InhibiTOR of Aging Emerges
622 From the Soil of Easter Island. *J Gerontol A Biol Sci Med Sci* 71: 841-849, 2016.
623 21. **Zhan JK, Wang YJ, Wang Y, Wang S, Tan P, Huang W, and Liu YS**. The mammalian
624 target of rapamycin signalling pathway is involved in osteoblastic differentiation of vascular
625 smooth muscle cells. *Can J Cardiol* 30: 568-575, 2014.
626 22. **He HQ, Law BYK, Zhang N, Qiu CL, Qu YQ, Wu AG, Han Y, Song Q, Zheng WL, Liu**
627 **Y, He YZ, and Wong VKW**. Bavachin Protects Human Aortic Smooth Muscle Cells Against
628 beta-Glycerophosphate-Mediated Vascular Calcification and Apoptosis via Activation of mTOR-
629 Dependent Autophagy and Suppression of beta-Catenin Signaling. *Front Pharmacol* 10: 1427,
630 2019.
631 23. **Dai XY, Zhao MM, Cai Y, Guan QC, Zhao Y, Guan Y, Kong W, Zhu WG, Xu MJ, and**
632 **Wang X**. Phosphate-induced autophagy counteracts vascular calcification by reducing matrix
633 vesicle release. *Kidney Int* 83: 1042-1051, 2013.

634 24. **Joolharzadeh P, and St Hilaire C**. CD73 (Cluster of Differentiation 73) and the
635 Differences Between Mice and Humans. *Arterioscler Thromb Vasc Biol* 39: 339-348, 2019.
636 25. **Ziegler SG, Ferreira CR, MacFarlane EG, Riddle RC, Tomlinson RE, Chew EY,**
637 **Martin L, Ma CT, Sergienko E, Pinkerton AB, Millan JL, Gahl WA, and Dietz HC**. Ectopic
638 calcification in pseudoxanthoma elasticum responds to inhibition of tissue-nonspecific alkaline
639 phosphatase. *Sci Transl Med* 9: 2017.
640 26. **Xin HB, Deng KY, Rishniw M, Ji G, and Kotlikoff MI**. Smooth muscle expression of
641 Cre recombinase and eGFP in transgenic mice. *Physiol Genomics* 10: 211-215, 2002.
642 27. **Sengupta S, Peterson TR, Laplante M, Oh S, and Sabatini DM**. mTORC1 controls
643 fasting-induced ketogenesis and its modulation by ageing. *Nature* 468: 1100-1104, 2010.
644 28. **Magee JA, Ikenoue T, Nakada D, Lee JY, Guan KL, and Morrison SJ**. Temporal
645 changes in PTEN and mTORC2 regulation of hematopoietic stem cell self-renewal and
646 leukemia suppression. *Cell Stem Cell* 11: 415-428, 2012.
647 29. **Liu M, Espinosa-Diez C, Mahan S, Du M, Nguyen AT, Hahn S, Chakraborty R,**
648 **Straub AC, Martin KA, Owens GK, and Gomez D**. H3K4 di-methylation governs smooth
649 muscle lineage identity and promotes vascular homeostasis by restraining plasticity. *Dev Cell*
650 56: 2765-2782 e2710, 2021.
651 30. **Wanjare M, Kuo F, and Gerecht S**. Derivation and maturation of synthetic and
652 contractile vascular smooth muscle cells from human pluripotent stem cells. *Cardiovasc Res* 97:
653 321-330, 2013.
654 31. **Zhang L, Yang C, Li J, Zhu Y, and Zhang X**. High extracellular magnesium inhibits
655 mineralized matrix deposition and modulates intracellular calcium signaling in human bone
656 marrow-derived mesenchymal stem cells. *Biochem Biophys Res Commun* 450: 1390-1395,
657 2014.
658 32. **Schneider CA, Rasband WS, and Eliceiri KW**. NIH Image to ImageJ: 25 years of
659 image analysis. *Nat Methods* 9: 671-675, 2012.
660 33. **Li Q, Price TP, Sundberg JP, and Uitto J**. Juxta-articular joint-capsule mineralization in
661 CD73 deficient mice: similarities to patients with NT5E mutations. *Cell Cycle* 13: 2609-2615,
662 2014.
663 34. **Martin KA, Rzucidlo EM, Merenick BL, Fingar DC, Brown DJ, Wagner RJ, and**
664 **Powell RJ**. The mTOR/p70 S6K1 pathway regulates vascular smooth muscle cell
665 differentiation. *Am J Physiol Cell Physiol* 286: C507-517, 2004.
666 35. **Marx SO, Jayaraman T, Go LO, and Marks AR**. Rapamycin-FKBP inhibits cell cycle
667 regulators of proliferation in vascular smooth muscle cells. *Circ Res* 76: 412-417, 1995.
668 36. **Martin KA, Merenick BL, Ding M, Fetalvero KM, Rzucidlo EM, Kozul CD, Brown DJ,**
669 **Chiu HY, Shyu M, Drapeau BL, Wagner RJ, and Powell RJ**. Rapamycin promotes vascular
670 smooth muscle cell differentiation through insulin receptor substrate-1/phosphatidylinositol 3-
671 kinase/Akt2 feedback signaling. *J Biol Chem* 282: 36112-36120, 2007.
672 37. **Cheung C, Bernardo AS, Trotter MW, Pedersen RA, and Sinha S**. Generation of
673 human vascular smooth muscle subtypes provides insight into embryological origin-dependent
674 disease susceptibility. *Nat Biotechnol* 30: 165-173, 2012.
675 38. **Skalli O, Pelte MF, Peclet MC, Gabbiani G, Gugliotta P, Bussolati G, Ravazzola M,**
676 **and Orci L**. Alpha-smooth muscle actin, a differentiation marker of smooth muscle cells, is
677 present in microfilamentous bundles of pericytes. *J Histochem Cytochem* 37: 315-321, 1989.
678 39. **Qi M, Zhang L, Ma Y, Shuai Y, Li L, Luo K, Liu W, and Jin Y**. Autophagy Maintains
679 the Function of Bone Marrow Mesenchymal Stem Cells to Prevent Estrogen Deficiency-Induced
680 Osteoporosis. *Theranostics* 7: 4498-4516, 2017.

681 40. **Sun X, Zheng Y, Xie L, Zhou Y, Liu R, Ma Y, Zhao M, and Liu Y**. Autophagy reduces
682 aortic calcification in diabetic mice by reducing matrix vesicle body-mediated IL-1beta release.
683 *Exp Cell Res* 432: 113803, 2023.
684 41. **Mizushima N, and Yoshimori T**. How to interpret LC3 immunoblotting. *Autophagy* 3:
685 542-545, 2007.
686 42. **Ganesh SK, and Subathra Devi C**. Molecular and therapeutic insights of rapamycin: a
687 multi-faceted drug from Streptomyces hygroscopicus. *Mol Biol Rep* 50: 3815-3833, 2023.
688 43. **Dobrin PB, and Mrkvicka R**. Failure of elastin or collagen as possible critical
689 connective tissue alterations underlying aneurysmal dilatation. *Cardiovasc Surg* 2: 484-488,
690 1994.
691 44. **Dobrin PB, Baker WH, and Gley WC**. Elastolytic and collagenolytic studies of arteries.
692 Implications for the mechanical properties of aneurysms. *Arch Surg* 119: 405-409, 1984.
693 45. **Rahkonen O, Su M, Hakovirta H, Koskivirta I, Hormuzdi SG, Vuorio E, Bornstein P,**
694 **and Penttinen R**. Mice with a deletion in the first intron of the Col1a1 gene develop age-
695 dependent aortic dissection and rupture. *Circ Res* 94: 83-90, 2004.
696 46. **Sabate M**. Sirolimus Versus Paclitaxel: Second Round. *JACC Cardiovasc Interv* 15:
697 780-782, 2022.
698 47. **Rouer M, Xu BH, Xuan HJ, Tanaka H, Fujimura N, Glover KJ, Furusho Y, Gerritsen**
699 **M, and Dalman RL**. Rapamycin limits the growth of established experimental abdominal aortic
700 aneurysms. *Eur J Vasc Endovasc Surg* 47: 493-500, 2014.
701 48. **Zhou B, Li W, Zhao G, Yu B, Ma B, Liu Z, Xie N, Fu Y, Gong Z, Dai R, Zhang X, and**
702 **Kong W**. Rapamycin prevents thoracic aortic aneurysm and dissection in mice. *J Vasc Surg* 69:
703 921-932 e923, 2019.
704 49. **Zhao Y, Zhao MM, Cai Y, Zheng MF, Sun WL, Zhang SY, Kong W, Gu J, Wang X,**
705 **and Xu MJ**. Mammalian target of rapamycin signaling inhibition ameliorates vascular
706 calcification via Klotho upregulation. *Kidney Int* 88: 711-721, 2015.
707 50. **Li L, Miano JM, Cserjesi P, and Olson EN**. SM22 alpha, a marker of adult smooth
708 muscle, is expressed in multiple myogenic lineages during embryogenesis. *Circ Res* 78: 188-
709 195, 1996.
710 51. **Krohn JB, Hutcheson JD, Martinez-Martinez E, Irvin WS, Bouten CV, Bertazzo S,**
711 **Bendeck MP, and Aikawa E**. Discoidin Domain Receptor-1 Regulates Calcific Extracellular
712 Vesicle Release in Vascular Smooth Muscle Cell Fibrocalcific Response via Transforming
713 Growth Factor-beta Signaling. *Arterioscler Thromb Vasc Biol* 36: 525-533, 2016.
714 52. **Tanemura M, Ohmura Y, Deguchi T, Machida T, Tsukamoto R, Wada H, Kobayashi**
715 **S, Marubashi S, Eguchi H, Ito T, Nagano H, Mori M, and Doki Y**. Rapamycin causes
716 upregulation of autophagy and impairs islets function both in vitro and in vivo. *Am J Transplant*
717 12: 102-114, 2012.
718 53. **Duan ZX, Tu C, Liu Q, Li SQ, Li YH, Xie P, and Li ZH**. Adiponectin receptor agonist
719 AdipoRon attenuates calcification of osteoarthritis chondrocytes by promoting autophagy. *J Cell*
720 *Biochem* 121: 3333-3344, 2020.
721 54. **Jono S, McKee MD, Murry CE, Shioi A, Nishizawa Y, Mori K, Morii H, and Giachelli**
722 **CM**. Phosphate regulation of vascular smooth muscle cell calcification. *Circ Res* 87: E10-17,
723 2000.
724 55. **Millan A, Lanzer P, and Sorribas V**. The Thermodynamics of Medial Vascular
725 Calcification. *Front Cell Dev Biol* 9: 633465, 2021.
726 56. **Frauscher B, Kirsch AH, Schabhuttl C, Schweighofer K, Ketszeri M, Pollheimer M,**
727 **Dragun D, Schroder K, Rosenkranz AR, Eller K, and Eller P**. Autophagy Protects From
728 Uremic Vascular Media Calcification. *Front Immunol* 9: 1866, 2018.

57. **Szwed A, Kim E, and Jacinto E**. Regulation and metabolic functions of mTORC1 and mTORC2. *Physiol Rev* 101: 1371-1426, 2021.
58. **Goncharova EA**. mTOR and vascular remodeling in lung diseases: current challenges and therapeutic prospects. *FASEB J* 27: 1796-1807, 2013.
59. **Guertin DA, Stevens DM, Thoreen CC, Burds AA, Kalaany NY, Moffat J, Brown M, Fitzgerald KJ, and Sabatini DM**. Ablation in mice of the mTORC components raptor, rictor, or mLST8 reveals that mTORC2 is required for signaling to Akt-FOXO and PKCalpha, but not S6K1. *Dev Cell* 11: 859-871, 2006.
60. **Schott A, Kluttig A, Mikolajczyk R, Greiser KH, Werdan K, Sedding D, and Nuding S**. Association of arterial stiffness and heart failure with preserved ejection fraction in the elderly population - results from the CARLA study. *J Hum Hypertens* 37: 463-471, 2023.
61. **Writing Group M, Lloyd-Jones D, Adams RJ, Brown TM, Carnethon M, Dai S, De Simone G, Ferguson TB, Ford E, Furie K, Gillespie C, Go A, Greenlund K, Haase N, Hailpern S, Ho PM, Howard V, Kissela B, Kittner S, Lackland D, Lisabeth L, Marelli A, McDermott MM, Meigs J, Mozaffarian D, Mussolino M, Nichol G, Roger VL, Rosamond W, Sacco R, Sorlie P, Roger VL, Thom T, Wasserthiel-Smoller S, Wong ND, Wylie-Rosett J, American Heart Association Statistics C, and Stroke Statistics S**. Heart disease and stroke statistics--2010 update: a report from the American Heart Association. *Circulation* 121: e46-e215, 2010.
62. **Allison MA, Ho E, Denenberg JO, Langer RD, Newman AB, Fabsitz RR, and Criqui MH**. Ethnic-specific prevalence of peripheral arterial disease in the United States. *Am J Prev Med* 32: 328-333, 2007.
63. **Allison MA, Budoff MJ, Nasir K, Wong ND, Detrano R, Kronmal R, Takasu J, and Criqui MH**. Ethnic-specific risks for atherosclerotic calcification of the thoracic and abdominal aorta (from the Multi-Ethnic Study of Atherosclerosis). *Am J Cardiol* 104: 812-817, 2009.
64. **Chaturvedi N, Bulpitt CJ, Leggetter S, Schiff R, Nihoyannopoulos P, Strain WD, Shore AC, and Rajkumar C**. Ethnic differences in vascular stiffness and relations to hypertensive target organ damage. *J Hypertens* 22: 1731-1737, 2004.
65. **D'Agostino RB, Jr., Burke G, O'Leary D, Rewers M, Selby J, Savage PJ, Saad MF, Bergman RN, Howard G, Wagenknecht L, and Haffner SM**. Ethnic differences in carotid wall thickness. The Insulin Resistance Atherosclerosis Study. *Stroke* 27: 1744-1749, 1996.
66. **Ali H, Zmuda JM, Cvejkus RK, Kershaw EE, Kuipers AL, Oczypok EA, Wheeler V, Bunker CH, and Miljkovic I**. Wnt Pathway Inhibitor DKK1: A Potential Novel Biomarker for Adiposity. *J Endocr Soc* 3: 488-495, 2019.
67. **Bild DE, Detrano R, Peterson D, Guerci A, Liu K, Shahar E, Ouyang P, Jackson S, and Saad MF**. Ethnic differences in coronary calcification: the Multi-Ethnic Study of Atherosclerosis (MESA). *Circulation* 111: 1313-1320, 2005.
68. **Budoff MJ, Nasir K, Mao S, Tseng PH, Chau A, Liu ST, Flores F, and Blumenthal RS**. Ethnic differences of the presence and severity of coronary atherosclerosis. *Atherosclerosis* 187: 343-350, 2006.
69. **Malhotra R, Nicholson CJ, Wang D, Bhambhani V, Paniagua S, Slocum C, Sigurslid HH, Lino Cardenas CL, Li R, Boerboom SL, Chen YC, Hwang SJ, Yao C, Ichinose F, Bloch DB, Lindsay ME, Lewis GD, Aragam JR, Hoffmann U, Mitchell GF, Hamburg NM, Vasan RS, Benjamin EJ, Larson MG, Zapol WM, Cheng S, Roh JD, O'Donnell CJ, Nguyen C, Levy D, and Ho JE**. Matrix Gla Protein Levels Are Associated With Arterial Stiffness and Incident Heart Failure With Preserved Ejection Fraction. *Arterioscler Thromb Vasc Biol* 42: e61-e73, 2022.

70. **Dalmeijer GW, van der Schouw YT, Magdeleyns EJ, Vermeer C, Verschuren WM, Boer JM, and Beulens JW**. Matrix Gla protein species and risk of cardiovascular events in type 2 diabetic patients. *Diabetes Care* 36: 3766-3771, 2013.
71. **Chirinos JA**. Matrix Gla Protein, Large Artery Stiffness, and the Risk of Heart Failure With Preserved Ejection Fraction. *Arterioscler Thromb Vasc Biol* 42: 223-226, 2022.
72. **Buss SJ, Muenz S, Riffel JH, Malekar P, Hagenmueller M, Weiss CS, Bea F, Bekeredjian R, Schinke-Braun M, Izumo S, Katus HA, and Hardt SE**. Beneficial effects of Mammalian target of rapamycin inhibition on left ventricular remodeling after myocardial infarction. *J Am Coll Cardiol* 54: 2435-2446, 2009.
73. **Gu J, Hu W, Song ZP, Chen YG, Zhang DD, and Wang CQ**. Rapamycin Inhibits Cardiac Hypertrophy by Promoting Autophagy via the MEK/ERK/Beclin-1 Pathway. *Front Physiol* 7: 104, 2016.
74. **Volkers M, Konstandin MH, Doroudgar S, Toko H, Quijada P, Din S, Joyo A, Ornelas L, Samse K, Thuerauf DJ, Gude N, Glembotski CC, and Sussman MA**. Mechanistic target of rapamycin complex 2 protects the heart from ischemic damage. *Circulation* 128: 2132-2144, 2013.
75. **Chakraborty AD, Kooiker K, Kobak KA, Cheng Y, Lee CF, Razumova M, Granzier HH, Regnier M, Rabinovitch PS, Moussavi-Harami F, and Chiao YA**. Late-life Rapamycin Treatment Enhances Cardiomyocyte Relaxation Kinetics and Reduces Myocardial Stiffness. *bioRxiv* 2023.
76. **Flynn JM, O'Leary MN, Zambataro CA, Academia EC, Presley MP, Garrett BJ, Zykovich A, Mooney SD, Strong R, Rosen CJ, Kapahi P, Nelson MD, Kennedy BK, and Melov S**. Late-life rapamycin treatment reverses age-related heart dysfunction. *Aging Cell* 12: 851-862, 2013.
77. **McMullen JR, Sherwood MC, Tarnavski O, Zhang L, Dorfman AL, Shioi T, and Izumo S**. Inhibition of mTOR signaling with rapamycin regresses established cardiac hypertrophy induced by pressure overload. *Circulation* 109: 3050-3055, 2004.
78. **Baghdadi M, Nespital T, Monzo C, Deelen J, Gronke S, and Partridge L**. Intermittent rapamycin feeding recapitulates some effects of continuous treatment while maintaining lifespan extension. *Mol Metab* 81: 101902, 2024.

FIGURE LEGENDS

Figure 1: Histological comparison of Matrix Gla Protein (MGP) mice arteries, medial and intimal calcification in human arteries. **A.** Histological sections of *Mgp*$^{-/-}$ mouse aorta, human tibial plaque and human coronary artery with atherosclerotic plaque, stained for calcification (Cal) using Von Kossa Staining. Scale Bars: human tissue 1 mm, mouse tissue 0.5 mm. **B.** Dot Blot Assay to identify MGP protein in *Mgp*$^{+/+}$, *Mgp*$^{+/-}$, and *Mgp*$^{-/-}$ mice. Results representative of n=3 per group. **C.** Representative immunofluorescence images of MGP protein in aortas from *Mgp*$^{+/+}$, Mgp$^{+/-}$ and *Mgp*$^{-/-}$ mice. Scale Bars: 100 µm. n=6 *Mgp*$^{+/+}$ vehicle, n=6 *Mgp*$^{-/-}$ vehicle. P value calculated using T-test. Data are shown as means ± SD.

Figure 2: Impact of rapamycin treatment on survival in Matrix Gla Protein (*Mgp*)-deficient mice. A. Graphic illustration of vehicle (DMSO) or rapamycin [5 mg/kg] treatment protocol**. B.** Kaplan-Meier analysis of overall survival in *Mgp*$^{+/+}$ and *Mgp*$^{-/-}$ mice treated with vehicle (Dimethyl sulfoxide; DMSO) or rapamycin (5mg/kg/week) for 90 days until natural death. n=7 *Mgp*$^{-/-}$ rapamycin, n=19 *Mgp*$^{-/-}$ vehicle, n=8 *Mgp*$^{+/+}$ rapamycin, n=5 *Mgp*$^{+/+}$ vehicle. Mantel-Cox test and Gehan-Breslow-wilcoxon test were used for curve comparison.

825
826 **Figure 3: Effect of rapamycin treatment on medial calcification in *Mgp*-deficient mice. A.**
827 Graphic illustration of vehicle (DMSO) or 5 mg/kg rapamycin treatment for 25 days in *Mgp*$^{+/+}$ and
828 *Mgp*$^{-/-}$ mice. **B.** Representative microCT measurement of axial and cross sections of *Mgp*$^{-/-}$ mice
829 aortas treated with vehicle or 5 mg/kg rapamycin, administered either once or three times a week
830 for 25 days. Scale bar 0.2 mm. n=4 *Mgp*$^{-/-}$ 1x rapamycin, n=10 *Mgp*$^{-/-}$ 3x rapamycin, n=12 *Mgp*
831 $^{-/-}$ vehicle **C.** Representative Von Kossa staining images of *Mgp*$^{+/+}$ and *Mgp*$^{-/-}$ mice aortas treated
832 with vehicle or rapamycin three times a week for 25 days. Scale bar 0.2 mm. n=10 *Mgp*$^{-/-}$
833 rapamycin, n=10 *Mgp*$^{-/-}$ vehicle, n=10 *Mgp*$^{+/+}$ rapamycin, n=10 *Mgp*$^{+/+}$ vehicle. **D.** Representative
834 immunofluorescent images of Runx2 on *Mgp*$^{+/+}$ and *Mgp*$^{-/-}$ mice aortas treated with vehicle or
835 rapamycin three times a week for 25 days. Scale bar 50 µm. n=10 *Mgp*$^{-/-}$ rapamycin, n=9 *Mgp*$^{-/-}$
836 vehicle, n=10 *Mgp*$^{+/+}$ rapamycin, n=10 *Mgp*$^{+/+}$ vehicle. Data are shown as means ± SD. P value
837 were calculated using One-way ANOVA with multiple comparisons test (Figure B) and Two-way
838 ANOVA with multiple comparisons test (Figures C, D).
839
840 **Figure 4: Histological structure of *Mgp*$^{+/+}$ and *Mgp*$^{-/-}$ mice aorta treated with vehicle or**
841 **rapamycin. A.** Representative Masson's Trichrome staining images of *Mgp*$^{+/+}$ and *Mgp*$^{-/-}$ mice
842 aortas treated with vehicle (Veh; DMSO) or rapamycin (RAPA; [5 mg/kg]) three times a week for
843 25 days. Collagen fiber structure in blue. Scale bar 0.2mm. **B.** Representative Picrosirius staining
844 images of collagen in *Mgp*$^{+/+}$ and *Mgp*$^{-/-}$ mice treated with vehicle or rapamycin three times a week
845 for 25 days. Scale bar: 100 µm. n=10 *Mgp*$^{-/-}$ rapamycin, n=10 *Mgp*$^{-/-}$ vehicle, n=10 *Mgp*$^{+/+}$
846 rapamycin, n=10 *Mgp*$^{+/+}$ vehicle. **C.** Representative Verhoeff-Van Gieson (VVG) staining images
847 of *Mgp*$^{+/+}$ and *Mgp*$^{-/-}$ treated with vehicle or rapamycin three times a week for 25 days. Elastin
848 tortuosity and breakage quantified. Scale bar 0.2mm. n=7 *Mgp*$^{-/-}$ rapamycin, n=8 *Mgp*$^{-/-}$ vehicle,
849 n=8 *Mgp*$^{+/+}$ rapamycin, n=9 *Mgp*$^{+/+}$ vehicle. **D.** Representative immunofluorescent images of
850 smooth muscle actin (SMA) and myosin heavy chain gene (MYH11) SMA on *Mgp*$^{+/+}$ and *Mgp*$^{-/-}$
851 mice aortas treated with vehicle or rapamycin three times a week. Scale bar 50 µm. n=10 *Mgp*$^{-/-}$
852 rapamycin, n=10 *Mgp*$^{-/-}$ vehicle, n=10 *Mgp*$^{+/+}$ rapamycin, n=10 *Mgp*$^{+/+}$ vehicle. **E.** Representative
853 immunofluorescent images of proliferation markers (ki67) on *Mgp*$^{+/+}$ and *Mgp*$^{-/-}$ mice aortas treated
854 with vehicle or rapamycin three times a week for 25 days. Scale bar 50 µm. n=10 *Mgp*$^{-/-}$
855 rapamycin, n=10 *Mgp*$^{-/-}$ vehicle, n=10 *Mgp*$^{+/+}$ rapamycin, n=10 *Mgp*$^{+/+}$ vehicle. Data are shown as
856 means ± SD. P value were calculated using Two-way ANOVA with multiple comparisons test.
857
858
859 **Figure 5: The effect of rapamycin treatment autophagy flux. A.** Representative
860 immunofluorescent images of LC3 on *Mgp*$^{+/+}$ and *Mgp*$^{-/-}$ mice aortas treated with vehicle (Veh;
861 DMSO) or rapamycin (RAPA; [5 mg/kg]) three times a week for 25 days. LC3 decreased with
862 rapamycin in *Mgp*$^{-/-}$ mice compared to the *Mgp*$^{+/+}$ mice. Scale bar 50 µm. n=9 *Mgp*$^{-/-}$ rapamycin,
863 n=10 *Mgp*$^{-/-}$ vehicle, n=10 *Mgp*$^{+/+}$ rapamycin, n=10 *Mgp*$^{+/+}$ vehicle. **B.** Smooth muscle cells from
864 *Mgp*$^{+/+}$ and *Mgp*$^{-/-}$ mice were treated with vehicle (DMSO) or rapamycin (200 μM) for 14 hours,
865 followed by the addition of bafilomycin (BafA, 100 μM), an autophagy inhibitor, for an additional
866 24 hours. Levels of LC3 (LC3-I and LC3-II) were quantified by western blot. Rapamycin treatment
867 increases the levels of LC3-II/LC3I and LC3-II protein in both *Mgp*$^{+/+}$ and *Mgp*$^{-/-}$ mice smooth
868 muscle cells. n=6 *Mgp*$^{-/-}$ rapamycin, n=6 *Mgp*$^{-/-}$ vehicle, n=6 *Mgp*$^{+/+}$ rapamycin, n=6 *Mgp*$^{+/+}$ vehicle.
869 Data are shown as means ± SD. P value were calculated using One-way ANOVA with multiple
870 comparisons test (Figure A) and Two-way ANOVA with multiple comparisons test (Figure B).
871
872 **Figure 6: Survival probability of Matrix Gla Protein (MGP)-deficient mice with Rictor and**
873 **Raptor knockouts in vascular smooth muscle cells (SMC). A.** *Mgp*$^{-/-}$ using Cre recombinase

874 that target the gene encoding Rictor in SMC, a protein involved in mTORC2 signaling pathways.
875 *Mgp*$^{-/-}$*;Rictor*$^{SMC-/-}$ (n=5) and *Mgp*$^{-/-}$*;Rictor*$^{SMC+/+}$ *(n=7)* . **B.** *Mgp*$^{-/-}$ using Cre recombinase that target
876 the gene encoding Raptor in SMC a protein involved in mTORC1 signaling pathways. *Mgp*$^{-/-}$
877 *;Raptor*$^{SMC+/+}$ (n=6), *Mgp*$^{-/-}$*;Raptor*$^{SMC-/-}$ (n=7), The presence or absence of Rictor, when combined
878 with MGP deficiency, does not significantly affect the lifespan of the mice. However, Raptor plays
879 a crucial role in the survival of MGP-deficient mice. Data are shown as means ± SD. Mantel-Cox
880 test and Gehan-Breslow-wilcoxon test were used for curve comparison.
881
882
883
884

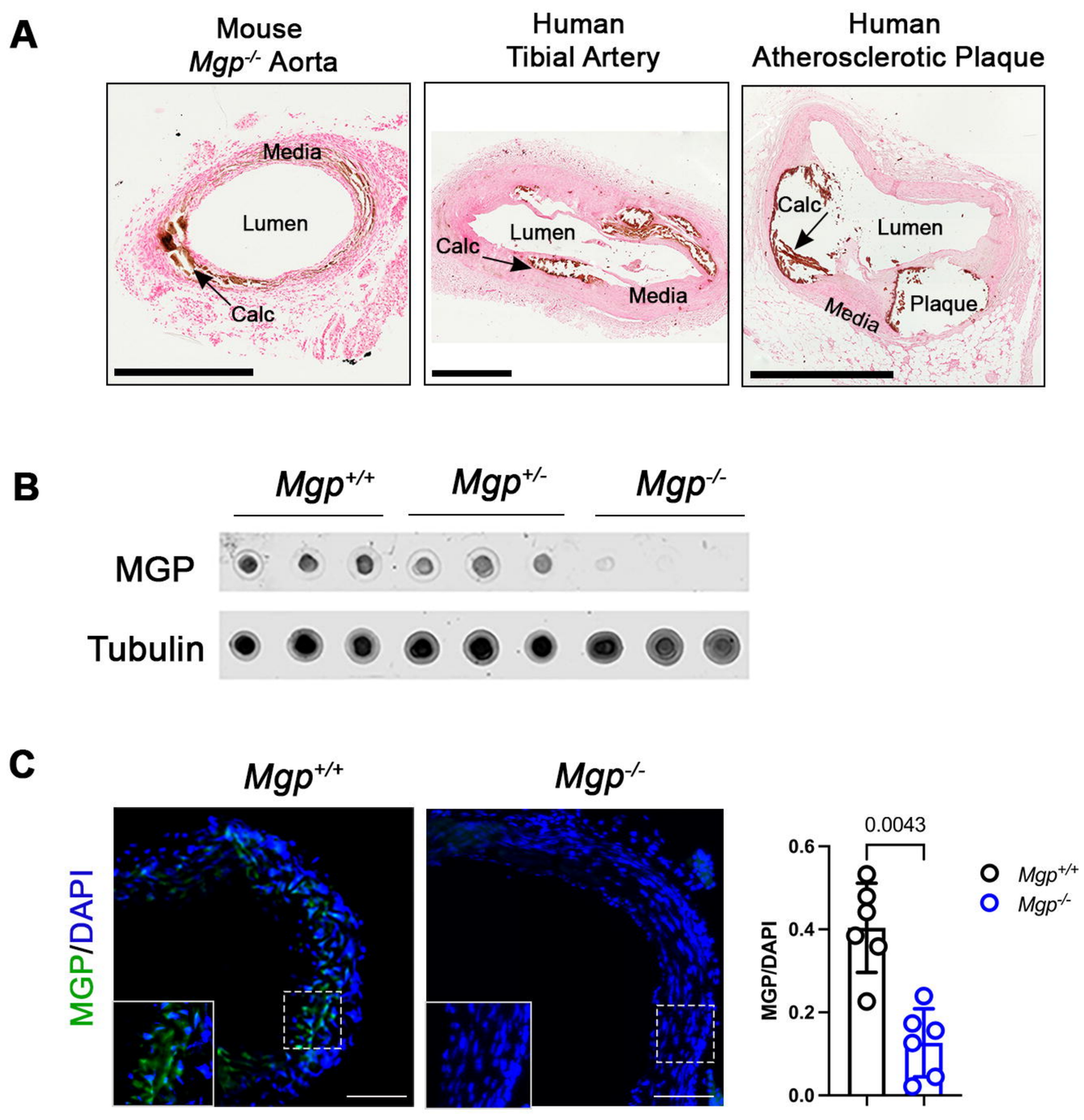
A
Mouse
Mgp-/- Aorta
Human
Tibial Artery
Human
Atherosclerotic Plaque
Media
Lumen
Calc
Lumen
Calc
Media
Calc
Lumen
Media
Plaque
B
Mgp+/+
Mgp+/-
Mgp-/-
MGP
Tubulin
C
Mgp+/+
Mgp-/-
MGP/DAPI
0.0043
0.6
0.4
0.2
0.0
MGP/DAPI
Mgp+/+
Mgp-/-

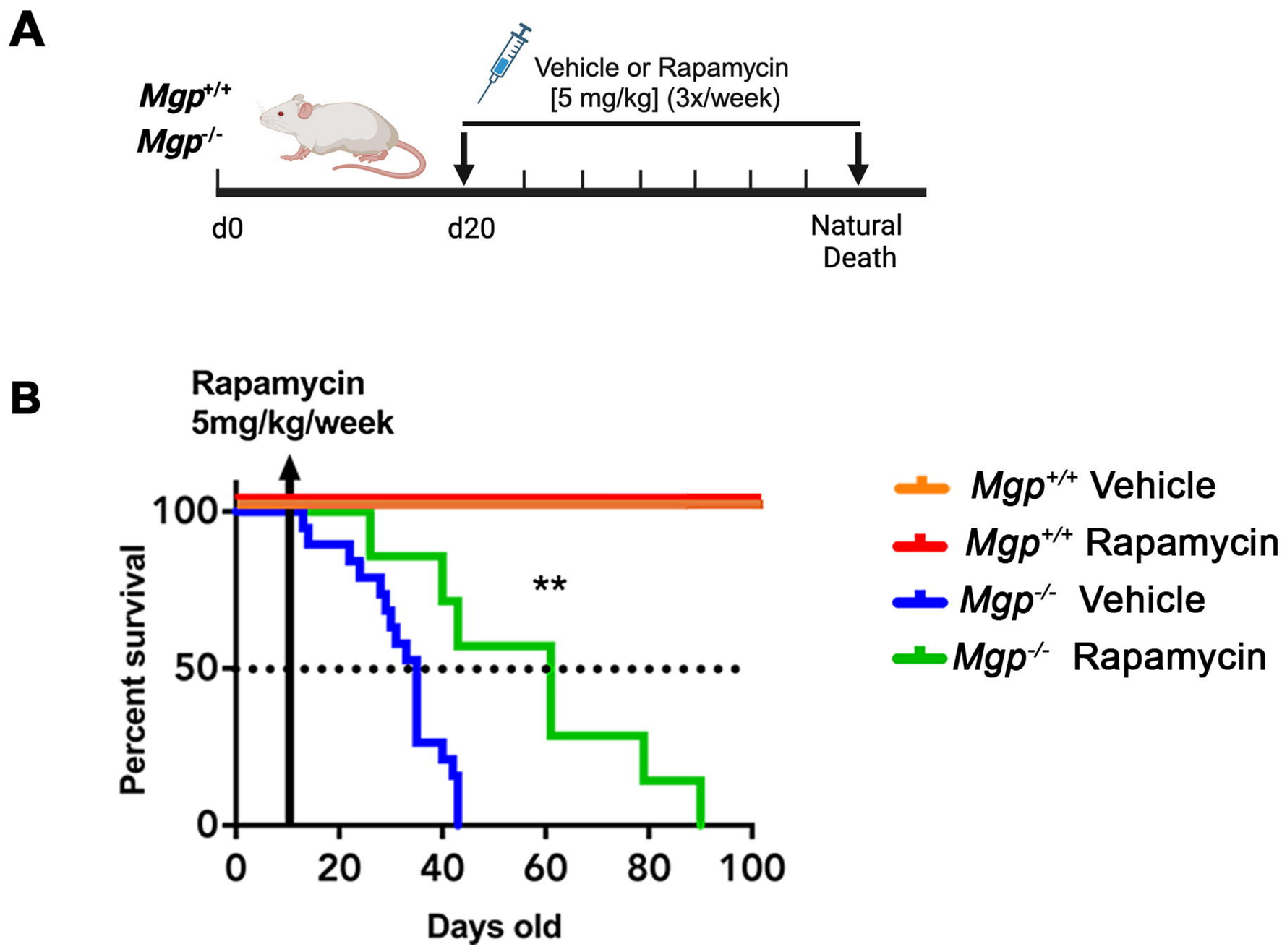
A
Mgp+/+
Mgp-/-
Vehicle or Rapamycin
[5 mg/kg] (3x/week)
d0
d20
Natural
Death
B
Rapamycin
5mg/kg/week
Percent survival
100
50
0
**
0
20
40
60
80
100
Days old
Mgp+/+ Vehicle
Mgp+/+ Rapamycin
Mgp-/- Vehicle
Mgp-/- Rapamycin

A

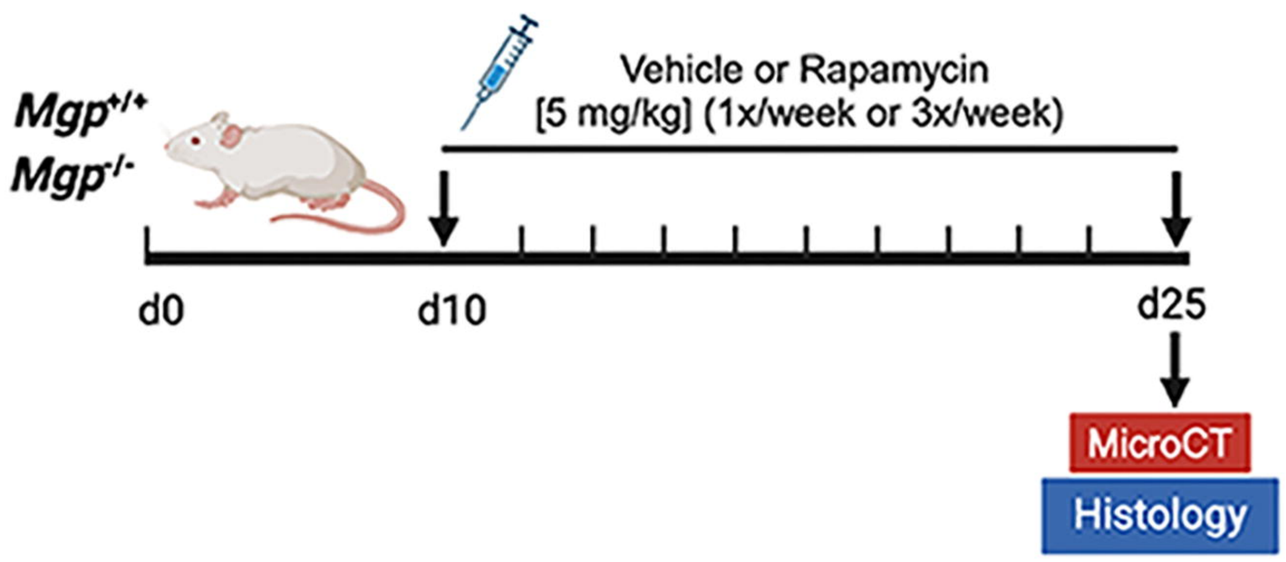
Mgp+/+
Mgp-/-
Vehicle or Rapamycin
[5 mg/kg] (1x/week or 3x/week)
d0
d10
d25
MicroCT
Histology

B

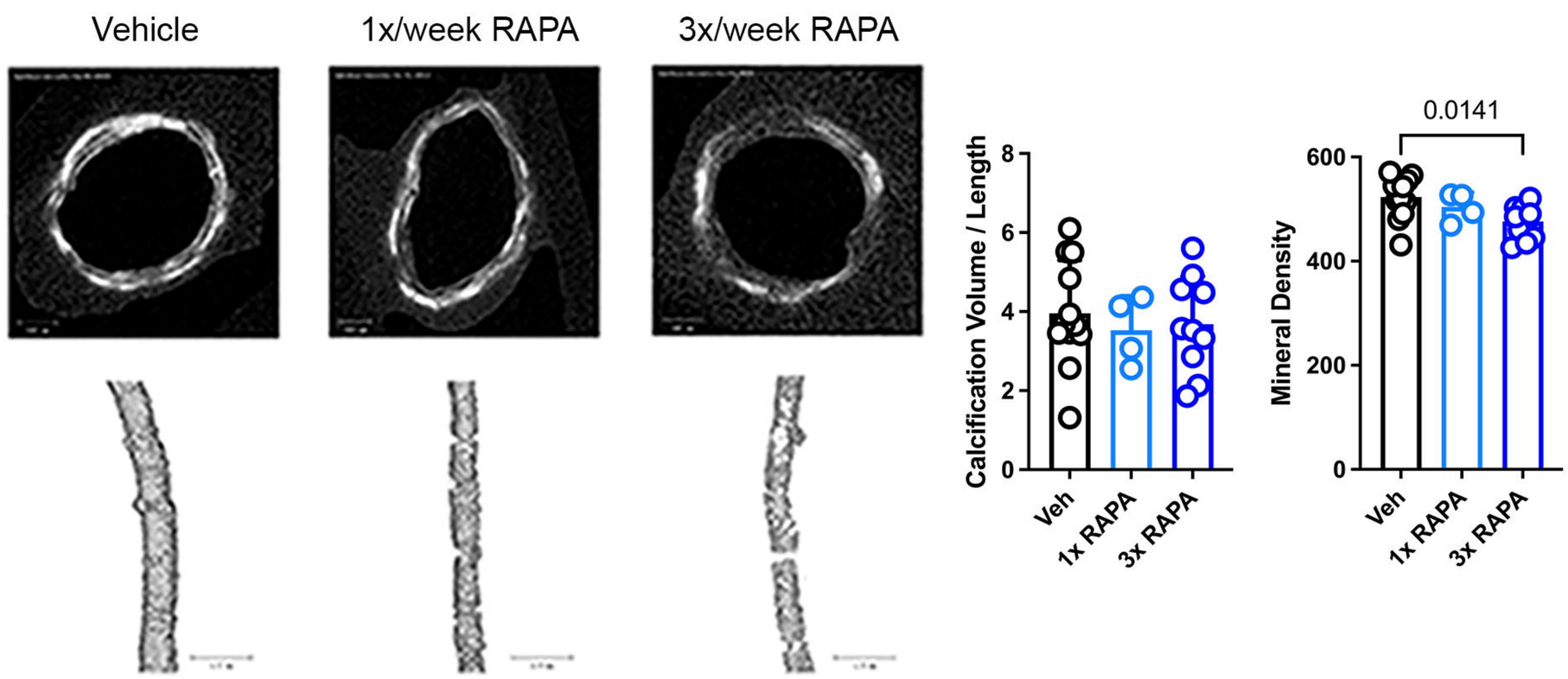
Vehicle
1x/week RAPA
3x/week RAPA
Calcification Volume / Length
Mineral Density
0.0141
Veh
1x RAPA
3x RAPA

C

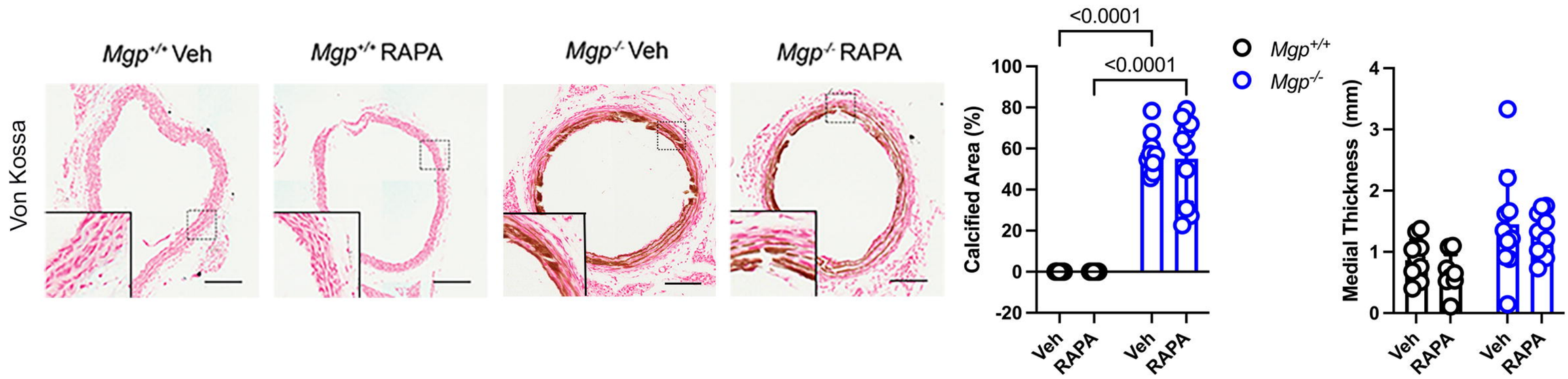
Mgp+/+ Veh
Mgp+/+ RAPA
Mgp-/- Veh
Mgp-/- RAPA
Von Kossa
Calcified Area (%)
<0.0001
<0.0001
Medial Thickness (mm)
Mgp+/+
Mgp-/-
Veh
RAPA

D

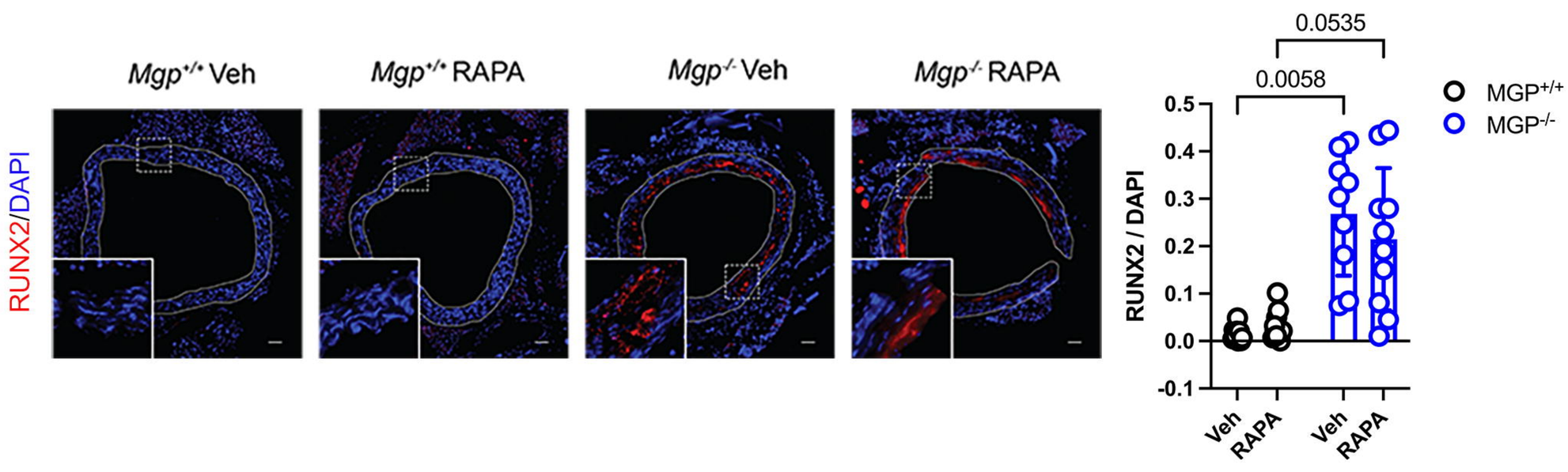
Mgp+/+ Veh
Mgp+/+ RAPA
Mgp-/- Veh
Mgp-/- RAPA
RUNX2/DAPI
RUNX2 / DAPI
0.0535
0.0058
MGP+/+
MGP-/-
Veh
RAPA

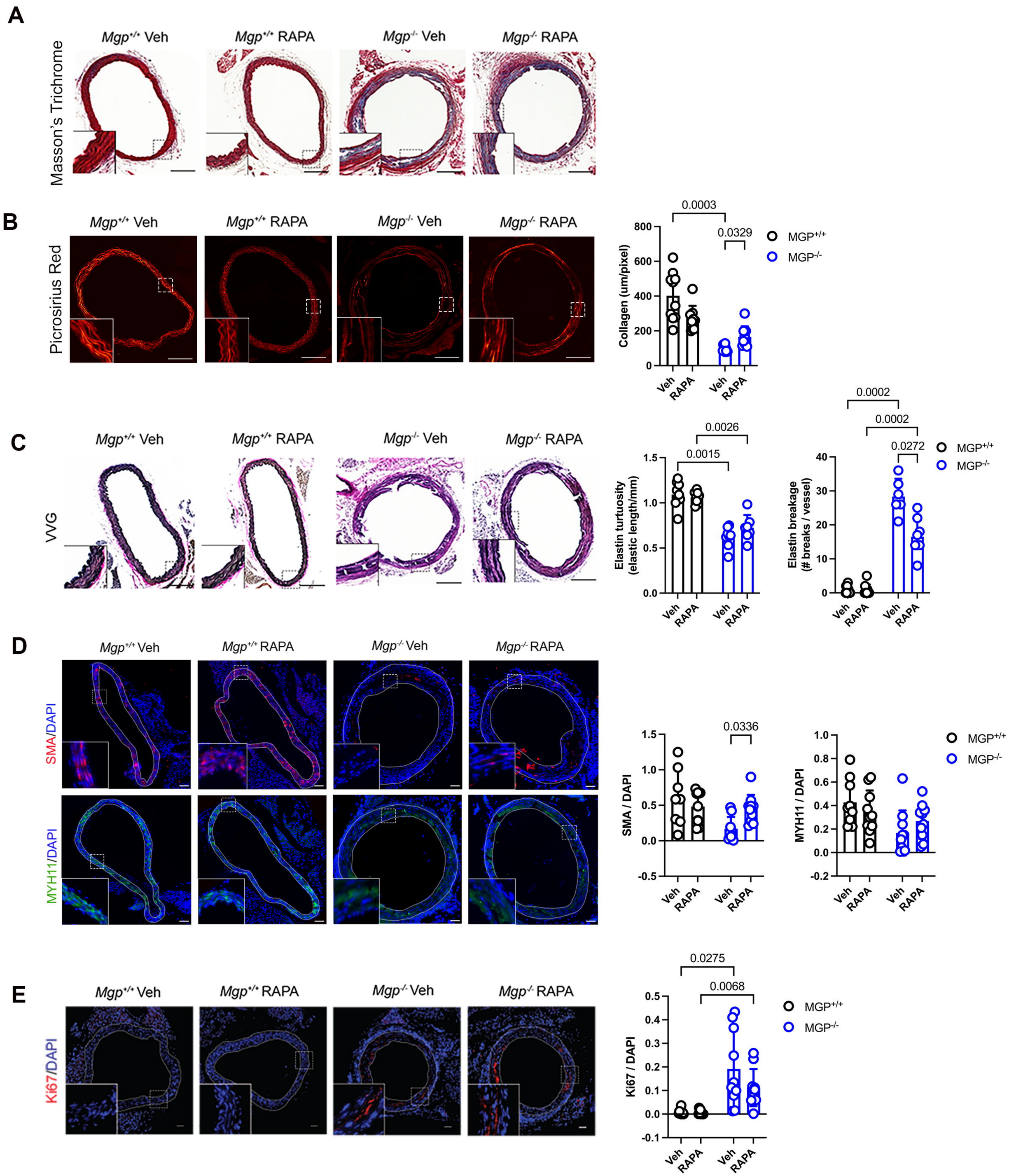
A
Mgp+/+ Veh
Mgp+/+ RAPA
Mgp-/- Veh
Mgp-/- RAPA
Masson's Trichrome
B
Picrosirius Red
Collagen (um/pixel)
0.0003
0.0329
MGP+/+
MGP-/-
Veh
RAPA
C
VVG
Elastin turtuosity (elastic length/mm)
0.0026
0.0015
Elastin breakage (# breaks / vessel)
0.0002
0.0002
0.0272
D
SMA/DAPI
MYH11/DAPI
SMA / DAPI
0.0336
MYH11 / DAPI
E
Ki67/DAPI
Ki67 / DAPI
0.0275
0.0068

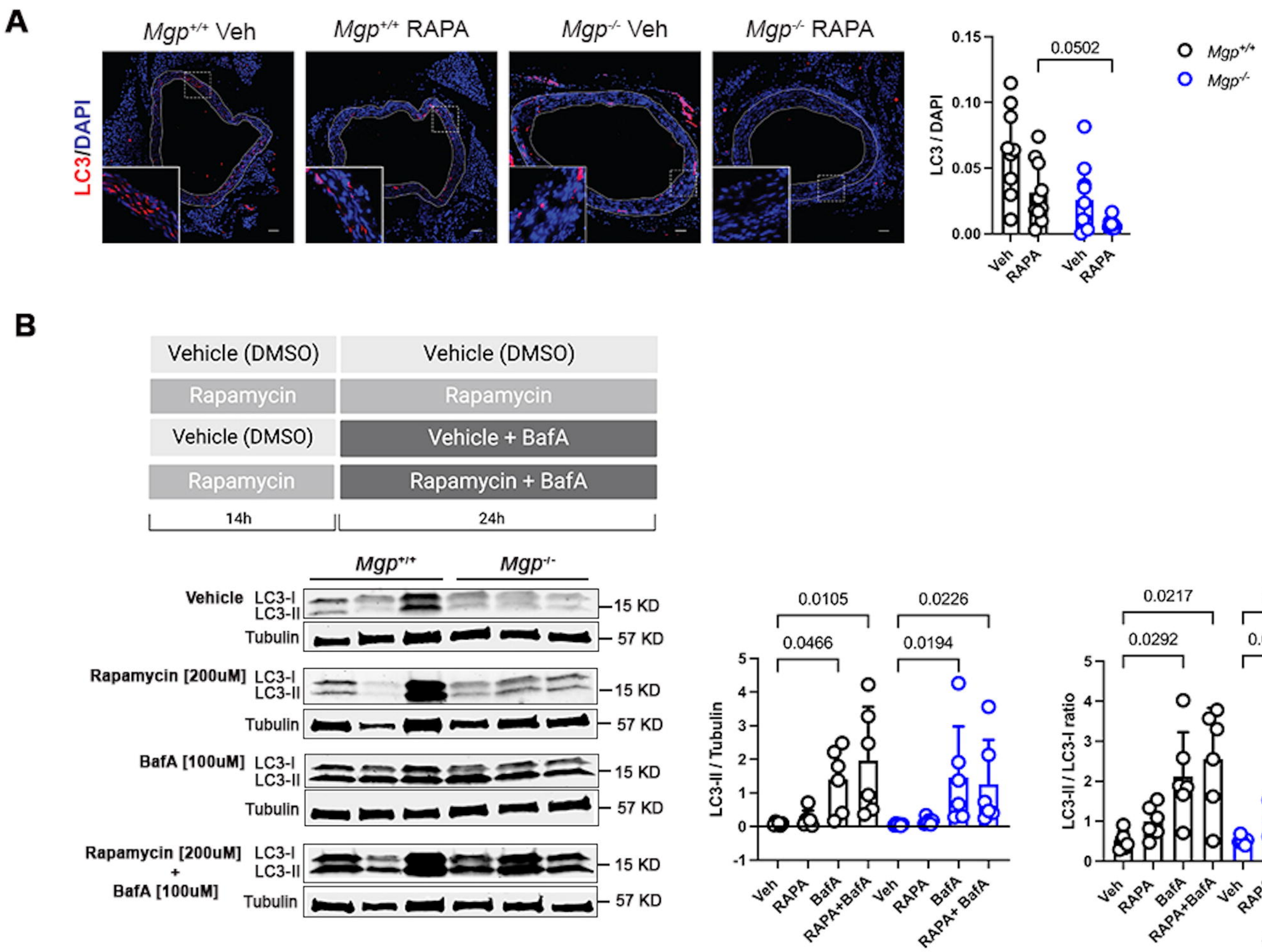
A
Mgp+/+ Veh
Mgp+/+ RAPA
Mgp-/- Veh
Mgp-/- RAPA
LC3/DAPI
LC3 / DAPI
0.15
0.10
0.05
0.00
0.0502
Veh
RAPA
Veh
RAPA
Mgp+/+
Mgp-/-
B
Vehicle (DMSO)
Vehicle (DMSO)
Rapamycin
Rapamycin
Vehicle (DMSO)
Vehicle + BafA
Rapamycin
Rapamycin + BafA
14h
24h
Mgp+/+
Mgp-/-
Vehicle
LC3-I
LC3-II
Tubulin
15 KD
57 KD
Rapamycin [200uM]
BafA [100uM]
Rapamycin [200uM] + BafA [100uM]
0.0105
0.0226
0.0466
0.0194
LC3-II / Tubulin
0.0217
0.0419
0.0292
0.0518
LC3-II / LC3-I ratio
Veh
RAPA
BafA
RAPA+BafA
RAPA+ BafA

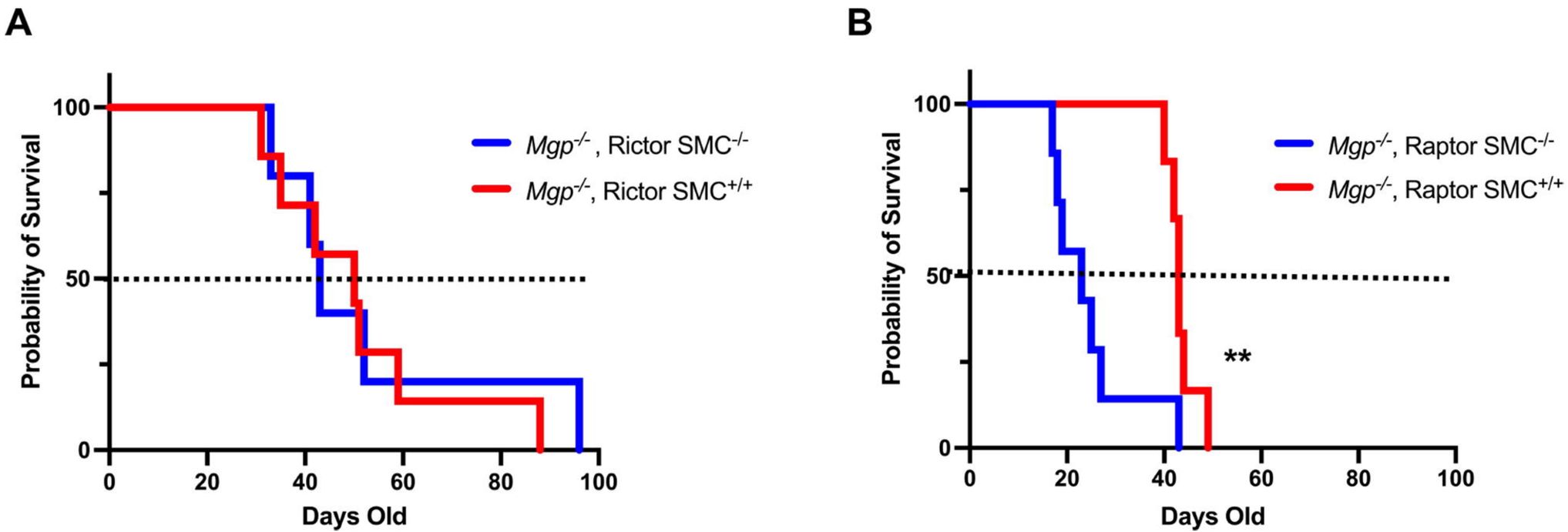
A
Probability of Survival
100
50
0
0
20
40
60
80
100
Days Old
Mgp-/-, Rictor SMC-/-
Mgp-/-, Rictor SMC+/+
B
Probability of Survival
100
50
0
0
20
40
60
80
100
Days Old
**
Mgp-/-, Raptor SMC-/-
Mgp-/-, Raptor SMC+/+

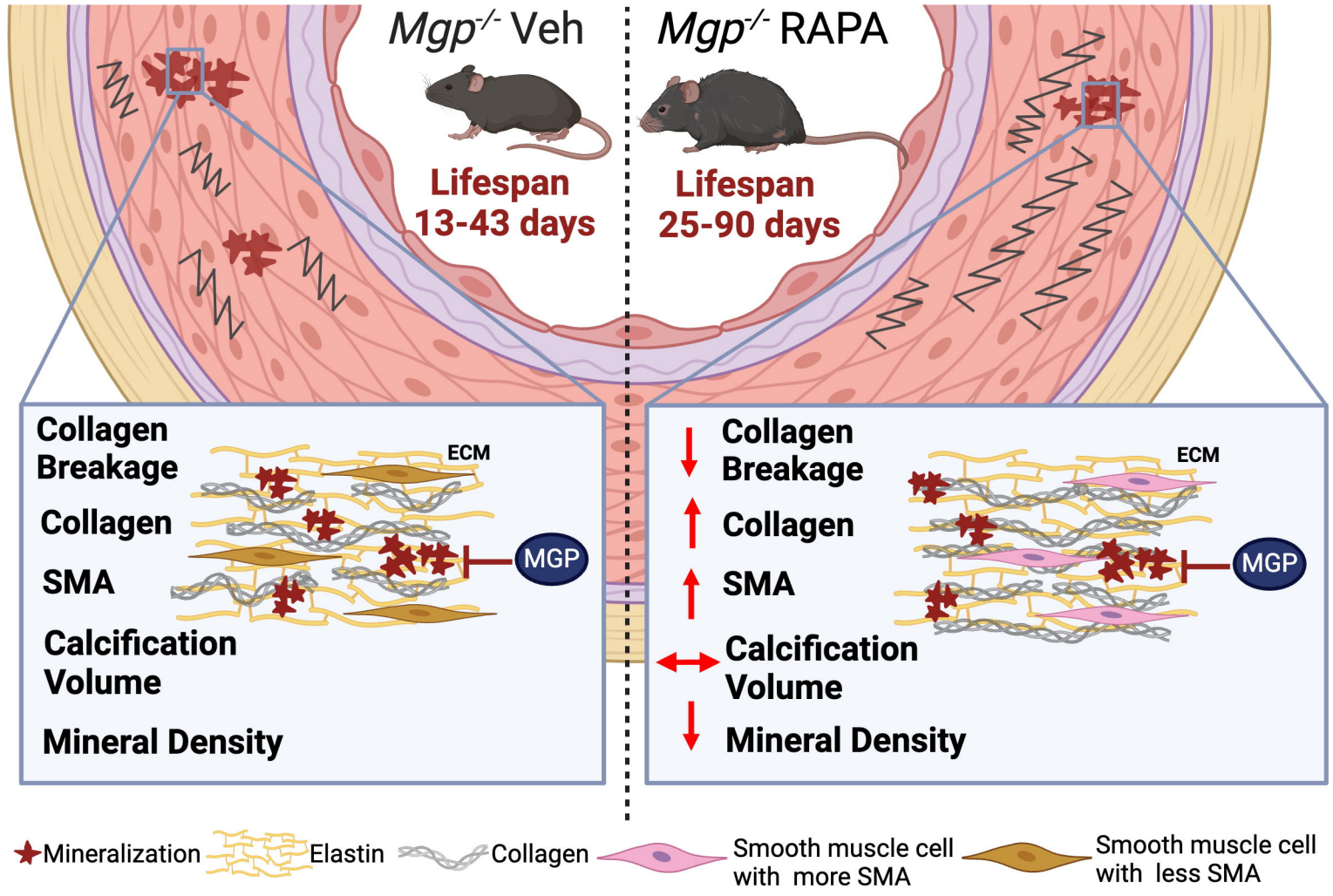

Matrix Gla protein (Mgp)-deficient mice develop extensive medial arterial calcification and die within 2 months of birth. We found that while treatment of these mice with rapamycin doubles their lifespan and improved the vascular structure. Vehicle (Veh), rapamycin (RAPA), Extracellular matrix (ECM), Smooth muscle alpha actin (SMA).